A progressive damage model for pressurized filament-wound hybrid composite pipe under low-velocity impact

Ammar Maziz, Mostapha Tarfaoui, Lokman Gemi, Said Rechak, Mourad Nachtane

A progressive damage model for pressurized filament-wound hybrid composite pipe under low-velocity impact

Ammar Maziz[1,2], Mostapha Tarfaoui[1], Lokman Gemi[3], Said Rechak[2], Mourad Nachtane[4]

[1]ENSTA Bretagne, IRDL, UMR CNRS 6027, F-29200 Brest, France

[2]Laboratoire GMD, ENP, El - Harrach, Algiers, Algeria

[3]Necmettin Erbakan University, Meram Vocational School, Konya, 42060, Turkey

[4]University of Bordeaux, CNRS, Arts et Metiers Institute of Technology, Bordeaux INP, INRAE, I2M Bordeaux, F-33400 Talence, France

*Corresponding Author: mostapha.tarfaoui@ensta-bretagne.fr, ammar.maziz@ensta-bretagne.org, lgemi@erbakan.edu.tr

Abstract

Pressurized hybrid composite pipe structures, produced by filament wound subjected to impact loads, were numerically investigated. A combined 3D-FE Model based on the use of interlaminar and intralaminar damage models is established. Intralaminar damages such as matrix cracking and fibre failures are predicted using 3D Hashin criteria, whereas interlaminar damage (delamination) was evaluated using cohesive zone elements. The damage model was coded and implemented as a user-defined material subroutine (VUMAT) for Abaqus/Explicit. Numerical results in the form of contact force, displacement and energy dissipated compare well with the experimental results. Predicted matrix damage in each cross-ply of hybrid composite pipe and delamination onset were also presented in this paper. The ability of this new 3D model to simulate the damage evolution in the full-scale pressurized hybrid composite pipe under low-velocity impact events were demonstrated throughout comparison with existing experimental results published.

Keywords: Filament winding, Hybrid composite pipes, Low-velocity impact, VUMAT, Failure criteria

1. Introduction

Composite pipe structures are used in many industrial applications. Their important aspect is in the distribution of fluids or fuels. When used on real applications, pipes structures are subjected to combined loading conditions: Internal pressure due to fluids or the form of liquid or gas and accidental impact loads due to environmental conditions or during a repair. The risk of damage in the major parts of cases is presented, which pushes many researchers to study the evolution of damage in the integrity of the tubular structure [1-19]. Up to our knowledge, the majority of the studies about progressive damage are based on experimental investigation, in addition, at this stage of research, there is no or little numerical comparative study of the damage in hybrid tubular structures when those structures are subjected to combined loads pressure and impact loads. Due to the high cost of carbon fibres, optimal configurations are investigated in reducing costs and saving sufficient resistance. Hybridization of various fibres is one of the widely used approaches to achieve this target ensuring adequate mechanical properties with a cost reduction. In this regard, glass fibre is the best option in terms of cost, availability, and nature of the treatment. The ability to predict the damage and behaviour of composite pipes is essential and indispensable for the design of pipelines. Therefore, it is necessary to analyse the initiation and evolution of the damage.

In the literature and the recent investigation, there are studies about damage evolution in the composite pipe [20-31]. Farhood et al. [25] have been experimentally conducted the hybridization effects on the compressive strength of carbon and glass fibre in filament-wound hybrid composite pipes, under both sections after and before impact events, it was observed a high fluctuation by the impact curves (i.e. force-displacement) with a rebounding impact response caused by greater damage severity on the samples, mainly due to the high impact energy and the absence of internal pressure on the tested samples. Gemi et al. [26] investigated the effect of stacking sequences in a pressurized hybrid composite pipe under low-velocity impact. A comparative study between three stratifications was studied, and the damage formation and delamination onset were discussed. Gemi et al. [32-34] in another work investigated the low-velocity impact response when the pipe combined and subjected to internal pressure. It is found that the increased internal pressure generates an increased range in the low-velocity impact response and progressive damage. The effects of hybridization and stacking sequence in various laminates have been reported [35-39]. The effects of impact damages of ±55° glass epoxy composite cylinders and the influences of scales and sizes on failure and dynamic responses have been reported [40-42]. Özbek et al. [43] investigated the intraplay hybrid glass-basalt fibre reinforced composite pipe produced by filament wound subjected to quasi-static compression, the crashworthiness response and the failure mode was analysed. Guo et al. [44] investigated the progressive damage of thin composite laminates subjected to low-velocity impact, after that, the samples were

exposed to compression-load; the experimental curves show the best agreement with numerical results. The effect of low-velocity impact on hybrid composite pipes structures is always stayed not perfectly understood and especially its numerical simulation is extremely complicated. Energy absorption characteristics in composites and hybrid composite materials used in marine energy under impact loading was investigated in [45-48]. Shi et al. [49] proposed a damage evolution model for predicting different scenarios in a circular plate subjected to low-velocity impact, the experimental data confronted with the numerical model, the numerical results show the best agreement. With the same data, Zhou et al. [50] employed another 3D finite element model based on a modified progressive damage model to evaluate the dynamic response and damage onset in cross-ply composite laminates under low-velocity impact. Both methods validate the experimental results. In another work, Zhou et al. [51] based on the first experimental results drop on the composite circular plate, for simulating multiple impacts using restart technique existed in Abaqus software, the effect of a repeated impact is discussed. An experimental and numerical investigation on the dynamic response of composite panels under hydroelastic impact loading and slamming impacts are reported in [52-54]. In previously published studies by the author, composite pipes in GCG stacking sequence were produced in [±75/±55/±45] configuration. Considering all the pressure values specified in ANSI/AWWA C950 standard, low velocity impact tests at 20J energy level were applied to the prestressed samples and the samples were subjected to fatigue test at 50% of the maximum burst pressure [30, 33]. In the study, post-impact damages were examined in detail and it was determined that the damage occurred in the composite pipe decreased as the pre-stress values increased. It was also reported that in low prestressed samples, delamination damage and intense other damage modes were observed in the impact region due to high displacement, while at high prestress values, only delamination damage was to occur. Pipes subjected to low-velocity impact under these conditions were subjected to fatigue test and it was determined that their fatigue life increased with the increase in pre-stress. In the study, burst tests were applied to the non-damaged pipes and pipes exposed to low velocity impact at 4, 8, 12 bar prestressing values. It was determined that their burst strength was 310, 239, 264 and 282 bar, respectively. It was also reported that the residual burst strength after low velocity impact increased depending on an increase in the prestressing [30].

Impacts can significantly reduce the residual strength of composite structures without necessarily leaving visible marks on the outer surface, for that the simulation of progressive damage in composite structures under low-velocity impact is more and more recommended for improving their structural integrity. The main objective is to develop a robust numerical model to accurately represent what is being observed in experimental investigation. Small damage can have a considerable effect on the durability of the structure composite materials.

An efficient study of these structures makes it possible to reduce uncertainties and risks; it is the best way to know opportunities for product success before getting started. A robust numerical model consists of replacing a large part of the real tests to decrease the number of physical tests required for certification. However, the models, as well as the computational methods used for the simulations, must have the confidence of the control authorities, this permit dimensioning as well as the composite structures intended to operate for a long time.

While there is no numerical analysis for hybrid composite pipe under low-velocity impact with variation in stacking sequences. In this present work, a 3D FE model simultaneously based on the application of interlaminar and intralaminar damage is constructed for simulating the impact-induced damage in a pressurized hybrid composite pipe at different stacking sequence, and comparing with existing experimental data published by Gemi et al. [26].

2. Constitutive Model of Damaged Material

In this section, the adoption of a progressive failure model in FE simulations was discussed. Damage on composite materials happens in two substantial steps namely: damage initiation and damage evolution. The damage onset and his propagation in hybrid laminate predicted and based on the continuum damage mechanics (CDM) to compute the coefficients degradation of the stiffness matrix, within this model, the relationship between the effective stress ($\hat{\sigma}$) and nominal stress (σ) for the damaged laminate, can be described in the form:

$$\hat{\sigma} = d.\sigma \tag{1}$$

Where d presents the damage operator.

Thus stress with the presence of the damages is given as:

$$\sigma_{i,j} = C_{i,j}\,(d).\,\varepsilon_{i,j} \tag{2}$$

Where C is the orthotropic stiffness matrix without damage. This matrix in the following form:

$$C = \begin{bmatrix} C_{11} & C_{12} & C_{13} & 0 & 0 & 0 \\ C_{12} & C_{22} & C_{23} & 0 & 0 & 0 \\ C_{13} & C_{23} & C_{33} & 0 & 0 & 0 \\ 0 & 0 & 0 & C_{44} & 0 & 0 \\ 0 & 0 & 0 & 0 & C_{55} & 0 \\ 0 & 0 & 0 & 0 & 0 & C_{66} \end{bmatrix} \tag{3}$$

Then the damage stiffness matrix is as follow [44]:

$$
\begin{aligned}
dC_{11} &= (1-d_f)\,E_1\,(1-v_{23}{}^2)\Gamma, & dC_{22} &= (1-d_f)\,(1-d_m)\,E_2(1-v_{13}{}^2)\Gamma \\
dC_{33} &= (1-d_f)\,(1-d_m)\,E_3\,(1-v_{21}{}^2)\Gamma, & dC_{12} &= (1-d_f)\,(1-d_m)\,E_1(v_{21}-v_{31}v_{23})\Gamma \\
dC_{23} &= (1-d_f)\,(1-d_m)\,E_2(v_{32}-v_{12}v_{31})\Gamma, & dC_{31} &= (1-d_f)\,(1-d_m)\,E_1(v_{31}-v_{21}v_{32})\Gamma \\
dC_{44} &= (1-d_f)\,(1-d_{mt}s_{mt})\,E_1\,(1-d_{mc}s_{mc})G_{12}, & dC_{55} &= (1-d_f)\,(1-d_{mt}s_{mt})\,E_1(1-d_{mc}s_{mc})G_{23} \\
dC_{66} &= (1-d_f)\,(1-d_{mt}s_{mt})\,E_1(1-d_{mc}s_{mc})G_{31},
\end{aligned}
\tag{4}
$$

Where the damage variables and Γ are given by equation 5 [44]:

$$
\begin{aligned}
d_f &= 1-(1-d_{ft})\,(1-d_{fc}) \\
d_m &= 1-(1-d_{mt})\,(1-d_{mc}) \\
\Gamma &= 1/(1-v_{12}{}^2-v_{23}{}^2-v_{13}{}^2-2\,v_{12}v_{23}v_{13})
\end{aligned}
\tag{5}
$$

Where d_f, d_m and d_s is the damage variables for the fibre, matrix and shear failure mode respectively.

2.1. Intralaminar failure criteria

To develop a high-fidelity model to capture the damage, the modelling must consider the different forms of damage occurring during the impact tests. The damage of the composite material is an accumulation of microscopic and macroscopic defects at the fibre, matrix and ply scales [55, 56]. In our knowledge, fibre and matrix damage can happen among a lamina and the onset of this damage takes place when applying stress in the hybrid composite laminate [34, 45], which ranges the highest strength of the oriented different stacking layers. Damage formation happens in the overall interface because of the difference between both moduli, the transverse compression modulus of the fibres and the modulus of the matrix, which shows the main reason for the initiation of damage. A developed user material VUMAT subroutine was coded in FORTRAN language and accomplished by the FE Abaqus/Explicit package, to compute the intralaminar damage. The failure initiation was identified, the events of damage formation were modelled (without ignoring the interlaminar mechanism) and are based on the use of 3D Hashin failure criteria [57, 58], for both case fibres and matrix and this criterion was used by many researchers and in the industrial field and provide a better result in the damage analysis of composite structures application. On the other hand, the main inconvenience of these criteria is the combination of different fracture mechanisms of the UD plies together. In the present study, these criteria are used in all procedure of progressive damage of the hybrid composite pipe and illustrated in Table 1.

Table 1. Hashin failure criteria [59].

Fibre Tensile Failure ($\sigma_{11} \geq 0$):	$f_{ft} = \left(\frac{\sigma_{11}}{X_t}\right)^2 \geq 1$
Fibre Compression Failure ($\sigma_{11} < 0$)	$f_{fc} = \left(\frac{\sigma_{11}}{X_c}\right)^2 \geq 1$
Matrix Tensile Failure ($\sigma_{22} + \sigma_{33}) \geq 0$	$f_{mt} = \frac{(\sigma_{22} + \sigma_{33})^2}{{Y_t}^2} + \frac{{\sigma_{23}}^2 - \sigma_{22}\sigma_{33}}{S_{23}^2} + \left(\frac{\sigma_{12}}{S_{12}}\right)^2 + \left(\frac{\sigma_{13}}{S_{13}}\right)^2 \geq 1$
Matrix Compression Failure ($\sigma_{22} + \sigma_{33}) < 0$	$f_{mc} = \frac{1}{Y_c}\left(\left(\frac{Y_c}{2S_{23}}\right)^2 - 1\right)(\sigma_{22} + \sigma_{33}) + \frac{(\sigma_{22} + \sigma_{33})^2}{4{S_{23}}^2} + \frac{{\sigma_{23}}^2 - \sigma_{22}\sigma_{33}}{S_{23}^2} + \left(\frac{\sigma_{12}}{S_{12}}\right)^2 + \left(\frac{\sigma_{13}}{S_{13}}\right)^2 \geq 1$

2.2. Damage evolution

As before mentioned, following the satisfaction of onset failure criteria, supplementary loading runs to degradation of composite material stiffness, consequently, the material properties were changed following model degradation of material property, determined by the relationship between the effective stress and displacement, the phase of damage formation evolution can be established. Also, the full variables of damage for each mode in both cases, the matrix and fibres are defined as displacement form:

$$d_i = \frac{\delta_{i,eq}^f(\delta_{i,eq} - \delta_{i,eq}^0)}{\delta_{i,eq}(\delta_{i,eq}^f - \delta_{i,eq}^0)} \quad , \quad \delta_{i,eq}^0 \leq \delta_{i,eq} \leq \delta_{i,eq}^f \tag{6}$$

δ_{eq}^0 : Equivalent displacements at the starting point of the damage.

$\delta_{i,eq}^f$: Equivalent displacements at the total propagated point of damage

$\delta_{i,eq}$: Equivalent displacement

d_i : Damage variable computed for each damage mode,

Therefore, as shown in Fig. 1, the point A and C correspond respectively to d=0 and d=1, and these different displacements can be calculated with the use of fracture energy relating to each variable of the damage as follows:

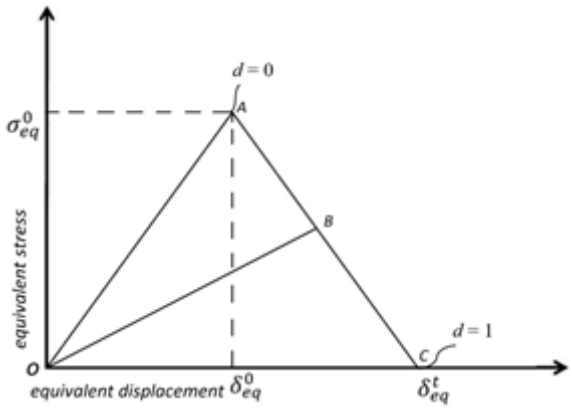

Fig. 1. Constitutive response of interlaminar damage model [45].

$$G_i = \int_{\delta^0_{i,eq}}^{\delta^f_{i,eq}} \sigma \, d\varepsilon = \frac{1}{2}\left(\delta^f_{i,eq} - \delta^0_{i,eq}\right)\sigma^0_{i,eq}$$

$$\delta^f_{i,eq} - \delta^0_{i,eq} = \frac{2G_i}{\sigma^0_{i,eq}} \tag{7}$$

$$\delta^0_{i,eq} = \delta_{i,eq}/\sqrt{f_i}$$

$$\sigma^0_{i,eq} = \sigma_{i,eq}/\sqrt{f_i}$$

$\sigma_{i,eq}$: equivalent stress

$\sigma^0_{i,eq}$: equivalent initial stress

f_i : initial failure

G_i : fracture energy

These variable corresponding to each mode, and each variable computed for each element's integration point, to define the degradation of stiffness in hybrid composite materials as illustrated in Table 2, therefore, in each iteration, the equivalent stress and equivalent displacements should be determined by the solver until the total failure reach's in elements d_f=1, consequently the model start to suppress elements, and the stress becomes a value of zero, in addition, the element will be deleted from the laminate stiffness [58].

Table 2. Equivalent displacement and equivalent stress presented for each mode [58].

Failure mode	$\boldsymbol{\delta_{i,eq}}$	$\boldsymbol{\sigma_{i,eq}}$
Fibre tensile damage mode	$L_c\sqrt{(\varepsilon_{11})^2 + (\varepsilon_{12})^2 + (\varepsilon_{31})^2}$	$L_c(\sigma_{11}\varepsilon_{11} + \sigma_{12}\varepsilon_{12} + \sigma_{31}\varepsilon_{31})/\delta_{1,eq}$
Fibre compressive damage mode	$L_c\sqrt{(-\varepsilon_{11} - \frac{\langle\varepsilon_{33}\rangle.\, E_{33}}{E_{11}})^2}$	$L_c(E_{11}(-\varepsilon_{11} - \frac{\langle\varepsilon_{33}\rangle.\, E_{33}}{E_{11}})/\delta_{2,eq}$
Matrix tensile damage mode	$L_c\sqrt{(\varepsilon_{22})^2 + (\varepsilon_{12})^2 + (\varepsilon_{23})^2}$	$L_c(\sigma_{22}\varepsilon_{22} + \sigma_{12}\varepsilon_{12} + \sigma_{23}\varepsilon_{23})/\delta_{3,eq}$
Matrix compressive damage mode	$L_c\sqrt{(-\varepsilon_{22} - \frac{\langle\varepsilon_{33}\rangle.\, E_{33}}{E_{22}})^2 + (\varepsilon_{12})^2}$	$L_c(E_{22}(-\varepsilon_{22} - \frac{\langle\varepsilon_{33}\rangle.\, E_{33}}{E_{22}} + \sigma_{12}\varepsilon_{12}\,)/\delta_{2,eq}$

Where $\langle\varepsilon_{ii}\rangle$ is the Macaulay operator and calculated as:

$$\langle\varepsilon_{ii}\rangle = \frac{\varepsilon_{ii} + |\varepsilon_{ii}|}{2} \tag{8}$$

L_c defined as characteristic length, which is determined when the material used exhibits strain-softening behaviour [57] to overcome the localisation of the strain, thus is integrated into the model to make the independence of the absorbed energy over model mesh sensitivity. In the 3D element case, the characteristic length is calculated by the cube root of the zone associated with the material point.

2.3. Interlaminar damage

Several simulation procedures use models of 3D behaviour that consider the effects of delamination in the same model, while others use the cohesive zone model because the plane of propagation of the delamination is located at the interface between two crossed orientations plies. For an accurate representation of the impacts scenario, it is important to establish adequate models. Inserting a cohesive interface into the modelling permits the prediction of interlaminar damage and its interaction with intralaminar damage. In the present work delamination onset between different layers of hybrid composite pipe was predicted by the implementation of the cohesive zone elements determined by a traction-separation law Fig. 2. This rule explains an initial linear-elastic phase until the satisfying the condition of the damage-initiation, subsequent by a linear phase of softening computing progressive de-cohesion of the cohesive interface with growing damage. In accordance with the law, the surface subjected to

the traction-displacement curve defines fracture toughness means the critical energy release rate for a particular fracture mode [60]. In this study, it is assumed that complete fracture occurs when the cohesive traction disappears at the final stage of the degradation phase. Damage evolution was controlled by an indicator of damage, varying from zero for undamaged elements until to reach the value equal to 1 pushing the total de-cohesion between layers. The crack onset occurred when a stress-based quadratic interaction criterion was satisfied:

$$\left(\frac{t_n}{t_n^{max}}\right)^2 + \left(\frac{t_s}{t_s^{max}}\right)^2 + \left(\frac{t_t}{t_t^{max}}\right)^2 \leq 1 \tag{9}$$

t_n , t_s and t_t represent the user elements cohesive stresses. Damage evolution was described using fracture energy, and a linear softening behaviour was employed. The fracture energy dependency on mixed fracture modes is described using Benzeggagh-Kenane formulation [61]:

$$G_C = G_C^I + (G_C^{II} - G_C^I)\left(\frac{G_C^{II} + G_C^{III}}{G_C^{II} + G_C^I}\right)^{\eta} \tag{10}$$

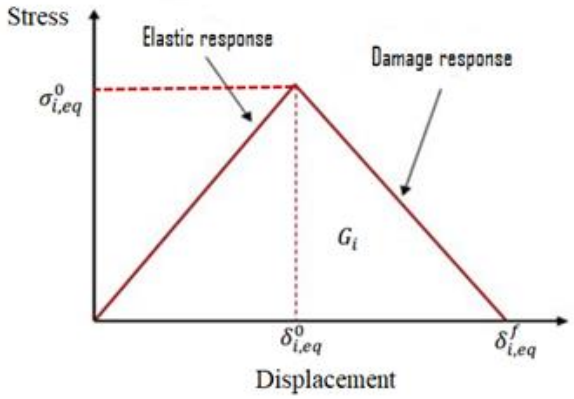

Fig. 2. Law of the traction-separation adopted for the CZM approach.

G_C^I , G_C^{II} and G_C^{III} relate to the crucial values of the energy of fracture necessary to incite the failure with each fracture mode.

For more demonstration, the algorithm of the proposed model is described in Fig. 3.

The simulations were performed using memory cluster system Linux workstation domain-level decomposition available in the MPI-based parallel solver of ABAQUS/Explicit was used for the computation.

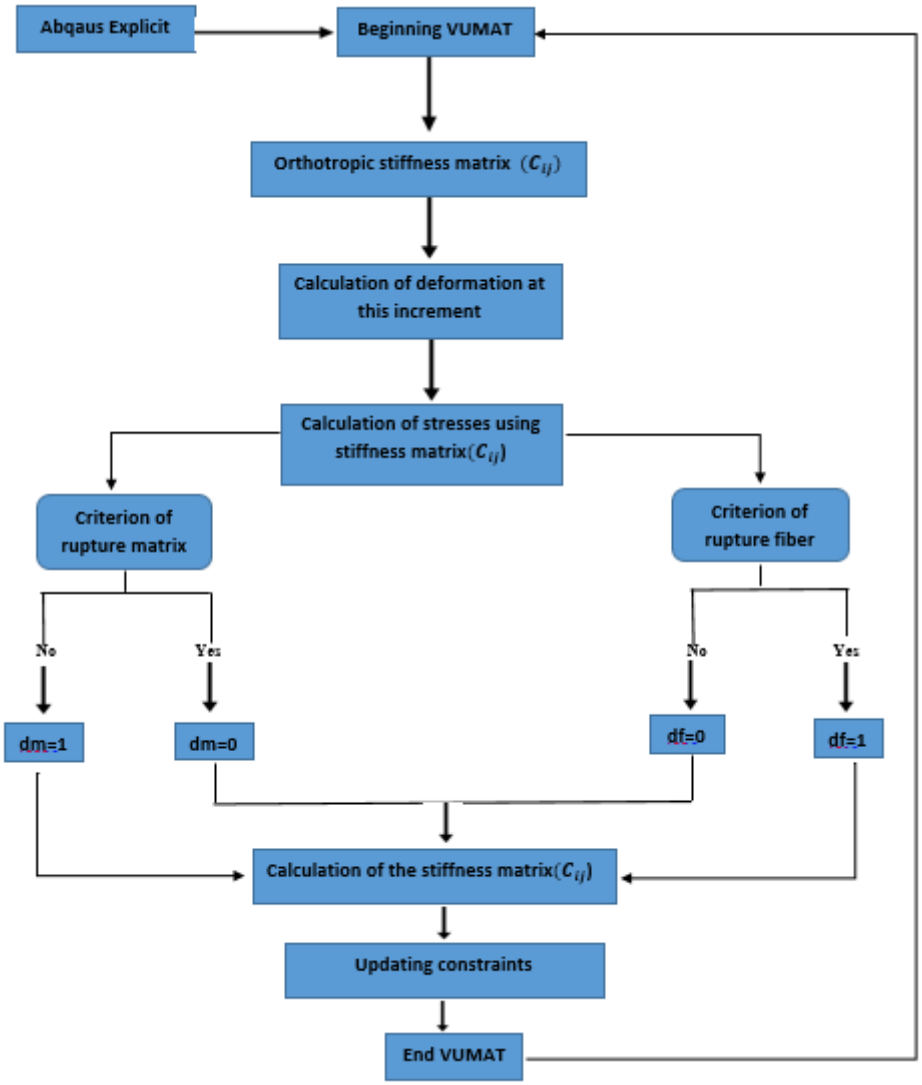

Fig. 3. Numerical implementation of the damage model (VUMAT) under Abaqus software

2.4. Material properties

To simulate the event of the pressurized hybrid composite pipe under low-velocity impact, the model of hybrid pipes consisted of different material properties, following the composite plies, and the parts such as the support and the impactor. In addition, cohesive interface properties are required. The properties of the stacking sequences were defined, based on the previous investigations [20, 21, 26] reported in Table 4, and the properties of three interfaces (carbon-carbon, glass carbon, glass-glass) have been defined by the inverse calculation and reported in Table 5.

Table 3. Geometry of the hybrid pipe

Internal radius, R_i (mm)	External radius, R_e (mm)	Tube length, L (mm)	Stacking sequence
36	38.4	300	$[\pm 55]_3$

Table 4: Material properties

Properties	Epoxy Matrix	E-Glass Fiber	Carbon Fiber
E (MPa)	3400	73100	230000
σ (MPa)	50-60	2345	3500
Fibre volume fraction (%)	-	50	10
Density (kg/m^3)	1200	2600	1750

Table 5: The cohesive contact model parameters

Interlaminar properties (Glass-Glass)	**Value**
Elastic (N/mm^3)	t_n =10, t_s =14, t_t = 14,
Strength (MPa)	$K_n = K_s = K_t$ = 1.00E +06,
Fracture (N/mm)	G_{IC}=0.145, G_{IIC}=0.2, G_{III}=0.2.
Mode Interaction BK	η =1.4.
Interlaminar properties (Carbon-Glass)	**Value**
Elastic (N/mm^3)	t_n =30, t_s =80, t_t = 80,
Strength (MPa)	$K_n = K_s = K_t$ =1.00E+06,
Fracture (N/mm)	G_{IC}=0.52 , G_{IIC}=0,97 ,G_{III}=0.97.
Mode Interaction BK	η =1.2.
Interlaminar properties (Carbon-Carbon)	**Value**
Elastic (N/mm^3)	t_n =20, t_s =80, t_t = 80,
Strength (MPa)	$K_n = K_s = K_t$ =1.00E+06,
Fracture (N/mm)	G_{IC}=0.512 , G_{IIC}=2,G_{III}=2.
Mode Interaction BK	η =1.3.

3. Boundary Conditions and Contact Algorithm

A 3D FE model was constructed for the analysis of composite hybrid pipe and to certify the prediction of the subroutine (VUMAT). The impactor, the stacking sequence, the support of V shape, and proper boundary conditions were applied as shown in Fig. 4. All boundary conditions have been defined in the numerical model according to the experimental tests investigated by Gemi [26]. For the contact algorithm, cohesive elements were

used between every two plies and hard contact between the support and the hybrid pipe [62]. The model constructed with a clamped edge. The hybrid composite pipes consisted of six plies oriented ±55° and each ply has a thickness of 0.4 mm, in this study an analysis of three stacking sequences is shown in Fig. 5. Total nodes of the hybrid composite pipe edge were attached in all direction x y z to compute the clamped conditions, Firstly an increment of internal pressure was defined in the load module and according to the experimental apparatus that it increases until to reach 32 bar before the contact between the impactor and the hybrid pipe, there are studies in the literature investigated the friction coefficient between composite and metal composite/composite [63, 64]. In the present study, a usual friction coefficient of 0.3, was employed for all of the introduced contacts (Hybrid pipe/support - Impactor/Hybrid pipe).

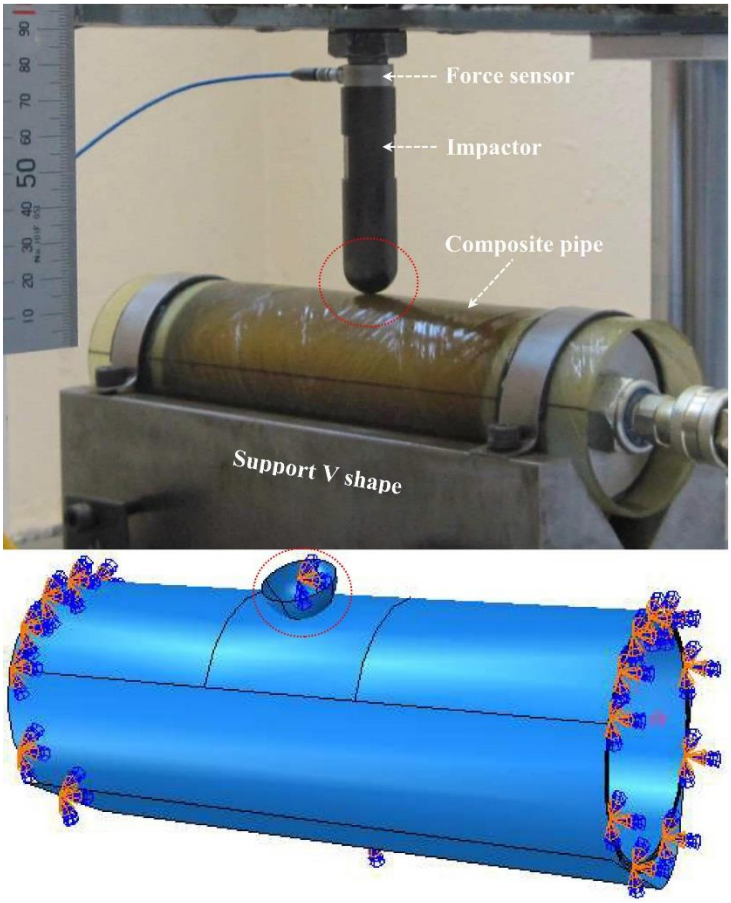

Fig. 4. Hybrid composite pipe under combined loads.

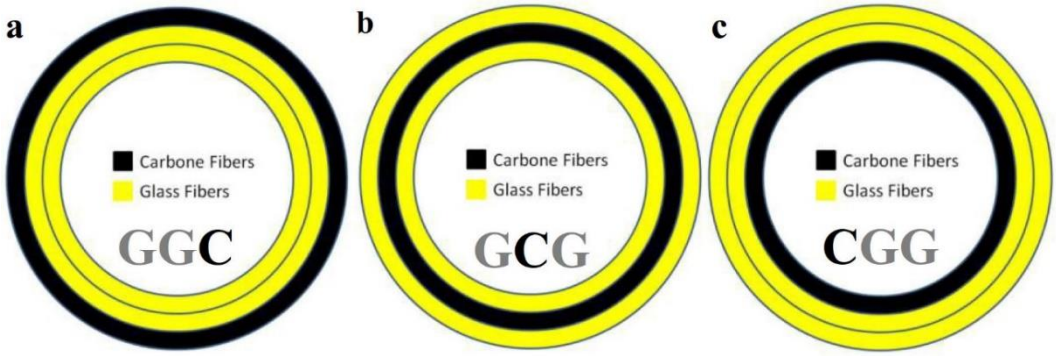

Fig. 5. Materials and stacking sequences

At the stage of determining the prestress value in the study, the studies conducted by the author [18, 26, 30, 32, 33], other studies in the literature [65, 66] and the operating pressures recommended by the ANSI/AWWA C950 standard [67, 68] were taken into consideration. According to the ANSI/AWWA C950 standard, operating pressures determined for GRP pipes are in the range of 4, 8, 12, 16, 20, 24, 28 and 32 bars. In this study, the prestressing pressure was chosen as the highest working pressure, 32 bar [26]. The undamaged burst tests of hybrid composite pipes were carried out in another study by the author, and as a result, the maximum burst stresses were obtained as 272, 280 and 265 bar in GGC, GCG and CGG stacked hybrid pipes, respectively [20].

3.1. Numerical implementation and mesh details

For a high-performance mesh, each ply was well discretized to consider out-of-plane stress components. All plies are meshed with linear volume elements C3D8R. The impactor that has a mass of 6.35 kg and the V shape support is modelled by rigid bodies and meshed with rigid quadrilateral elements R3D4. Cohesive zone elements were inserted between two full-scale plies, with zero mm in the thickness of the hybrid composite pipe and the inserted element technique in the interaction module of Abaqus was adopted [62]. The simulation is carried out by an explicit code simulation package. The generated mesh considered that the element's dimensions, size are identical. The distortion controls implemented in Abaqus software and the hourglass method using the enhanced scheme were employed for all of the elements [62]. According to the experimental device, it is imposed an initial condition as an impact speed at the affected reference point of the impactor. The condition of contact between the full impactor and the target does not allow inter-penetration between surfaces. To make sure good representation of the bending of the hybrid composite pipe, an enrichment by five integration points was performed in each average ply thickness. To minimize the calculation time without affecting the results of the simulation, an optimal mesh size, verifying the convergence of the numerical solution with the elastic phase is conducted. We start to reduce the element size from 10 mm, to 0.5 mm. As evidenced by the evolution, the convergence study in terms

of velocity and the impactor displacement during contact is shown in Figs. 6 and 7, where it is observed the 1 and 0.5 mm elements are identical.

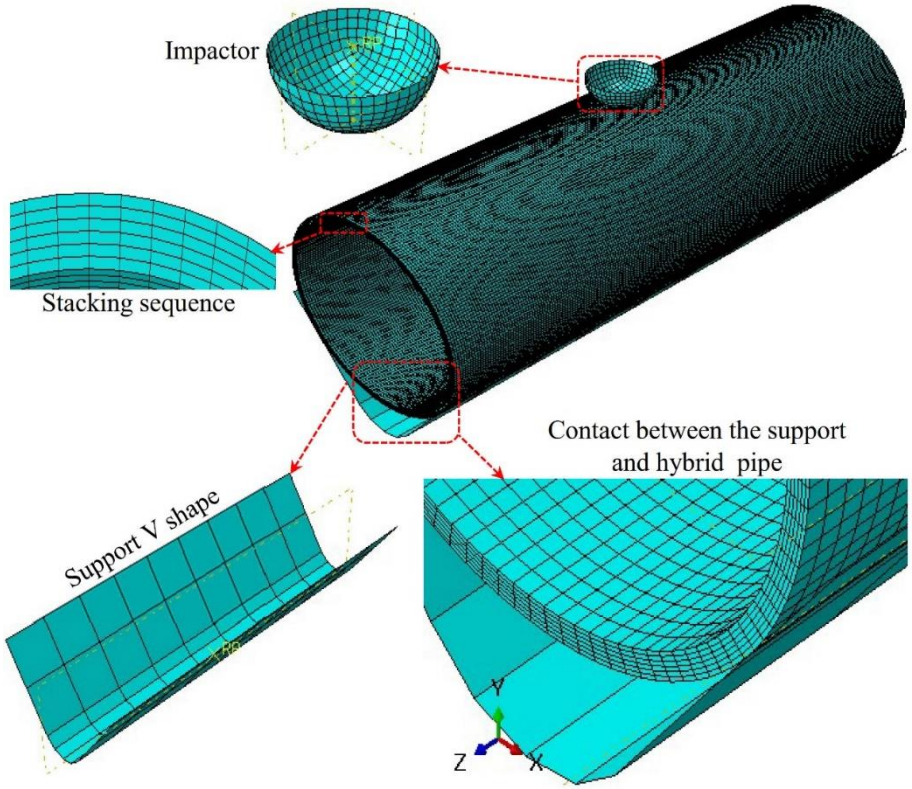

Fig. 6. Finite element model of full-scale hybrid pipes, impactor, and the support

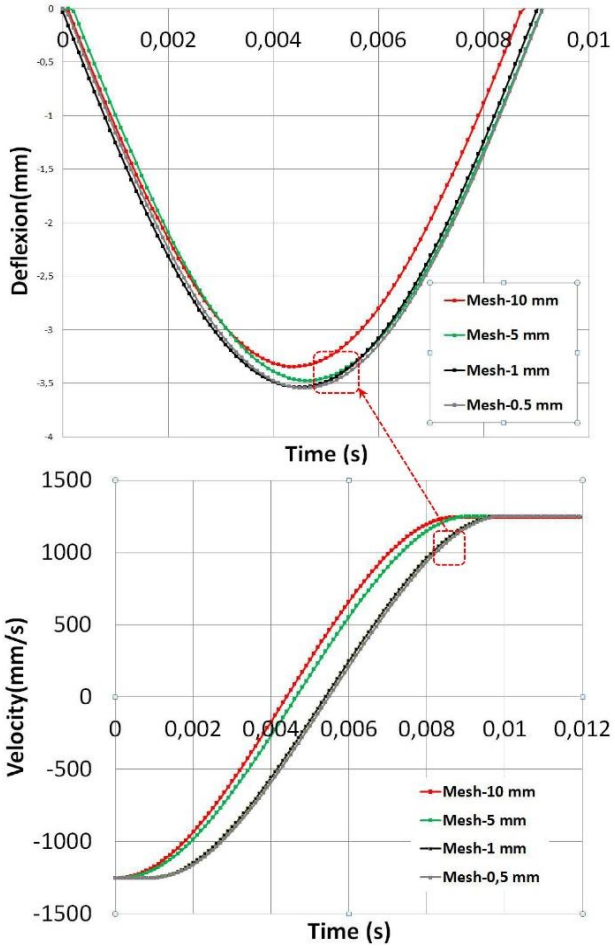

Fig. 7. Mesh convergence

4. Results and Discussion

To determine the impact velocity and energies to be applied to the pipes produced with the filament winding method in similar diameter and configuration, the literature reviewed comprehensively. Produced by the filament winding method, were investigated in determining the loading energies. In literature, researchers generally utilized 5, 10, 15, and 20J energy [69-74] and 1.5, 2, 2.5, and 3 m/s contact velocity [75-77] in the low-velocity impact test of composite pipes [78-79]. Damage analyses of FRP pipes, which were pre-damaged in these energy and speed ranges, were made and the remaining strength values after impact were determined. The low-velocity impact energies to be applied in the experimental stage of this study were determined based on the previous studies considering the diameter, thickness and number of layers of the pipe, and damage analysis after preliminary impact tests. Low-velocity impact tests were performed at 5, 10, 15, 20J energy level under 32 bar internal pressure for the hybrid pipes produced in three different stacking sequence. After the tests, damage developments were examined and the obtained results were presented comparatively. Based on the experimental study results, the present numerical study was developed and the results were compared with the experimental study and commented comparatively.

Following the convergence study, the obtained numerical results, are thus confronted with experimental curves data. The 3D model estimated the force-time loading curve for different stacking sequences. The variations and the maximum load values obtained from combined load events are presented in Figs. 8, 9 and 10. Through the impact results, the impactor drops on the hybrid pipe, and the contact force achieves the supreme value. Subsequently, the load decreases. It can be seen from the results that the variation of the load-time for each case of stacking sequences of pressurized hybrid pipe under the same impact energy is different. The cause rationale for this discrepancy is based is that the impact response of the hybrid composite pipes changes according to the different materials of stacking sequences. In addition, the fluctuations informed to be the symptom of progressive damage and these fluctuations increase with increasing the impact energy. Therefore, the model analyses provide approximately the same frequencies and peak-to-peak magnitudes as the data of experimental investigation, especially for the low impact energies of 5 and 10J (stacking sequences CGG and GCG). As seen in the experimental investigation [26] the samples show the same variation in temporal evolution, except for GGC stacking at 20J, the main cause is that the five and six layers of the GGC samples are hidden with the carbon fibre area which is impacted with very significant contact stress and the formation of damage during contact become easy. Therefore, it can be seen, in the stacking CGG and GCG that, the carbon plies are covered by glass plies that mean a decrease of stress compared GGC stacking. This correlation makes it possible to verify the adequacy of the developed model with the experimental results. For impact energies, 15J and 20J, the discrepancies between the experimental and the numerical results in unloading have observed which are attributed to the fact that the accuracy of the finite element analysis decreases with an increase in impact velocity. Moreover, the impactor would move slower in stacking sequence GGC, resulting in a longer duration. In general, the similar incidences and approximately peak to peak amplitude as the test curves in the experimental investigation for the different low impact energies.

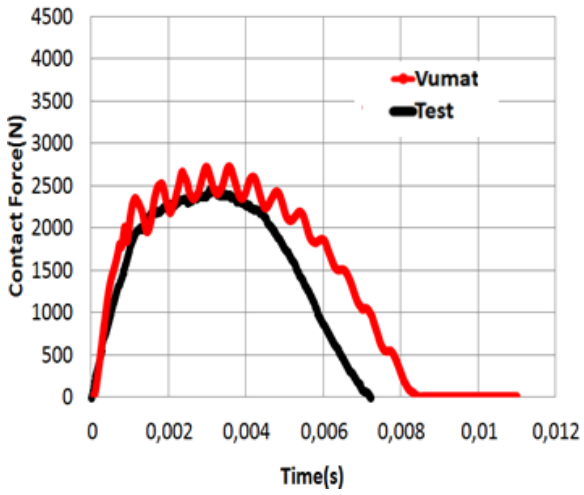

(a) 5J

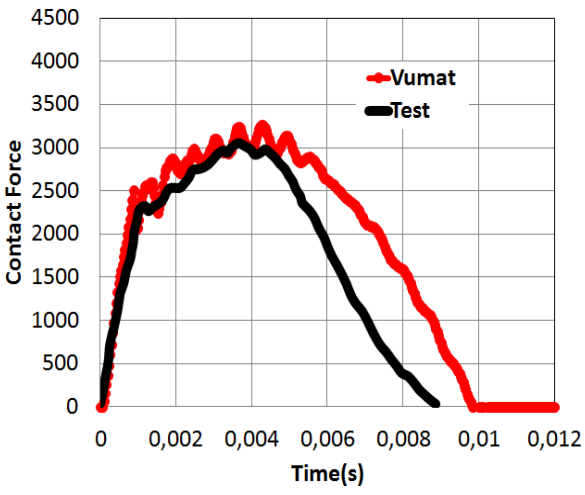

(b) 10J

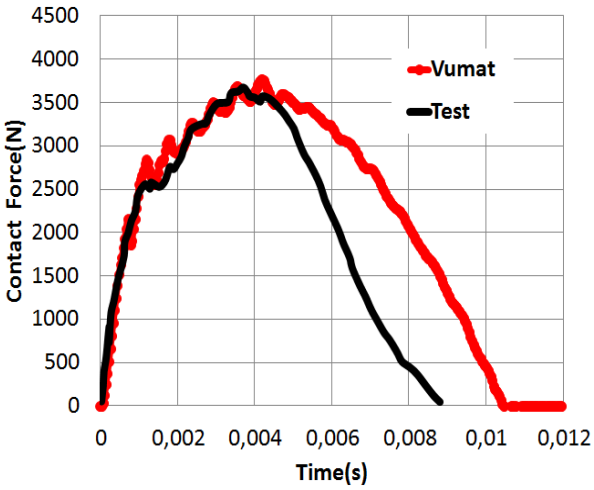

*(c)*15J

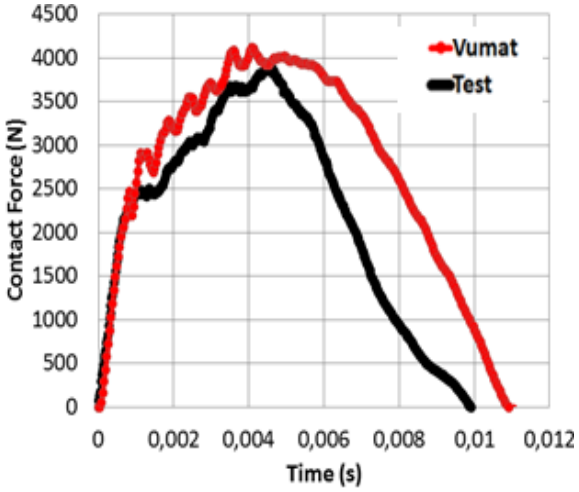

(d) 20J

Fig. 8. Confrontation Test/3D simulation of contact force-time curves of stacking sequences CGG under different impact energy

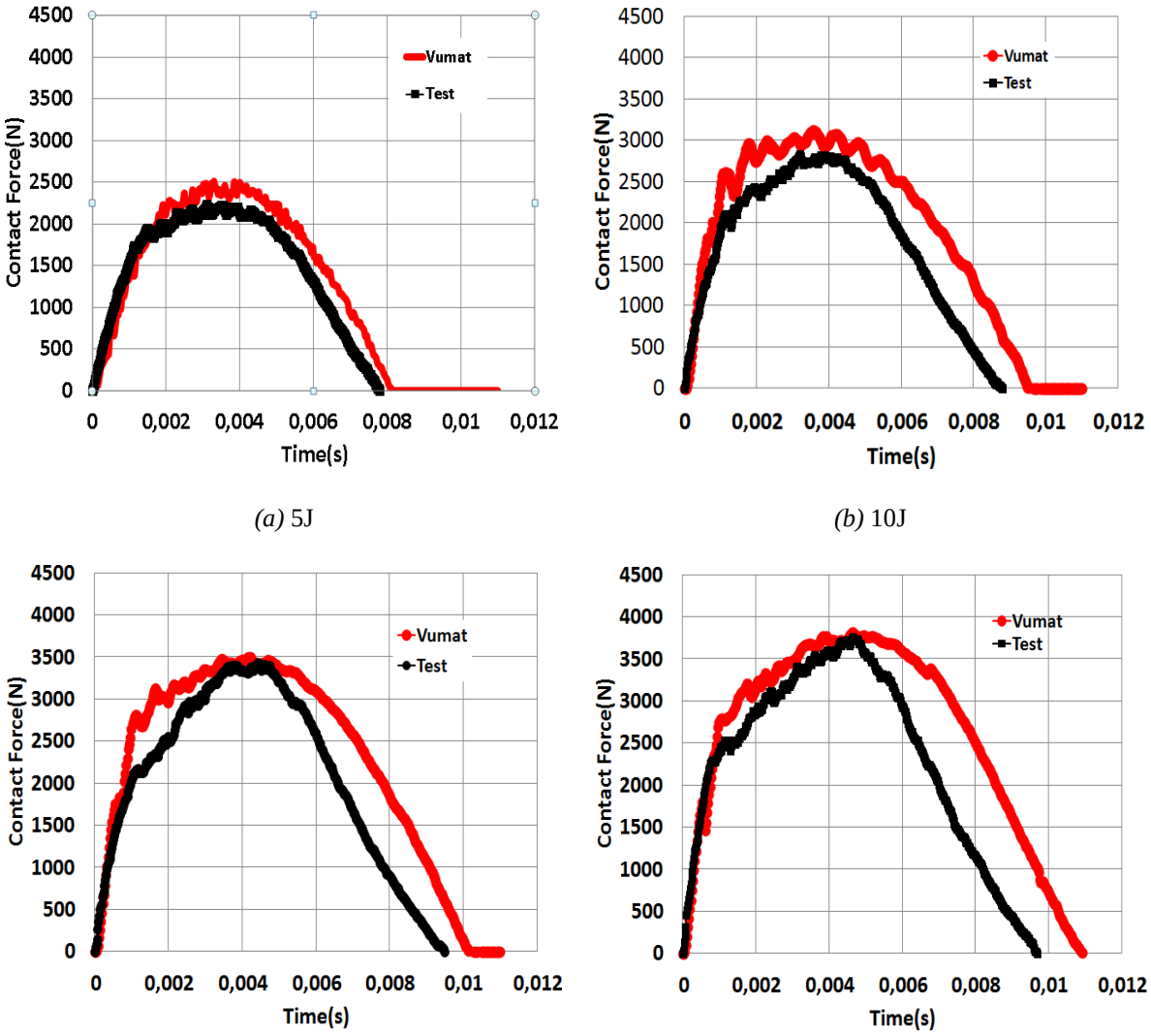

(a) 5J

(b) 10J

(c) 15J

(d) 20J

Fig. 9. Confrontation Test/3D simulation of contact force-time curves of stacking sequences GCG under different impact energy

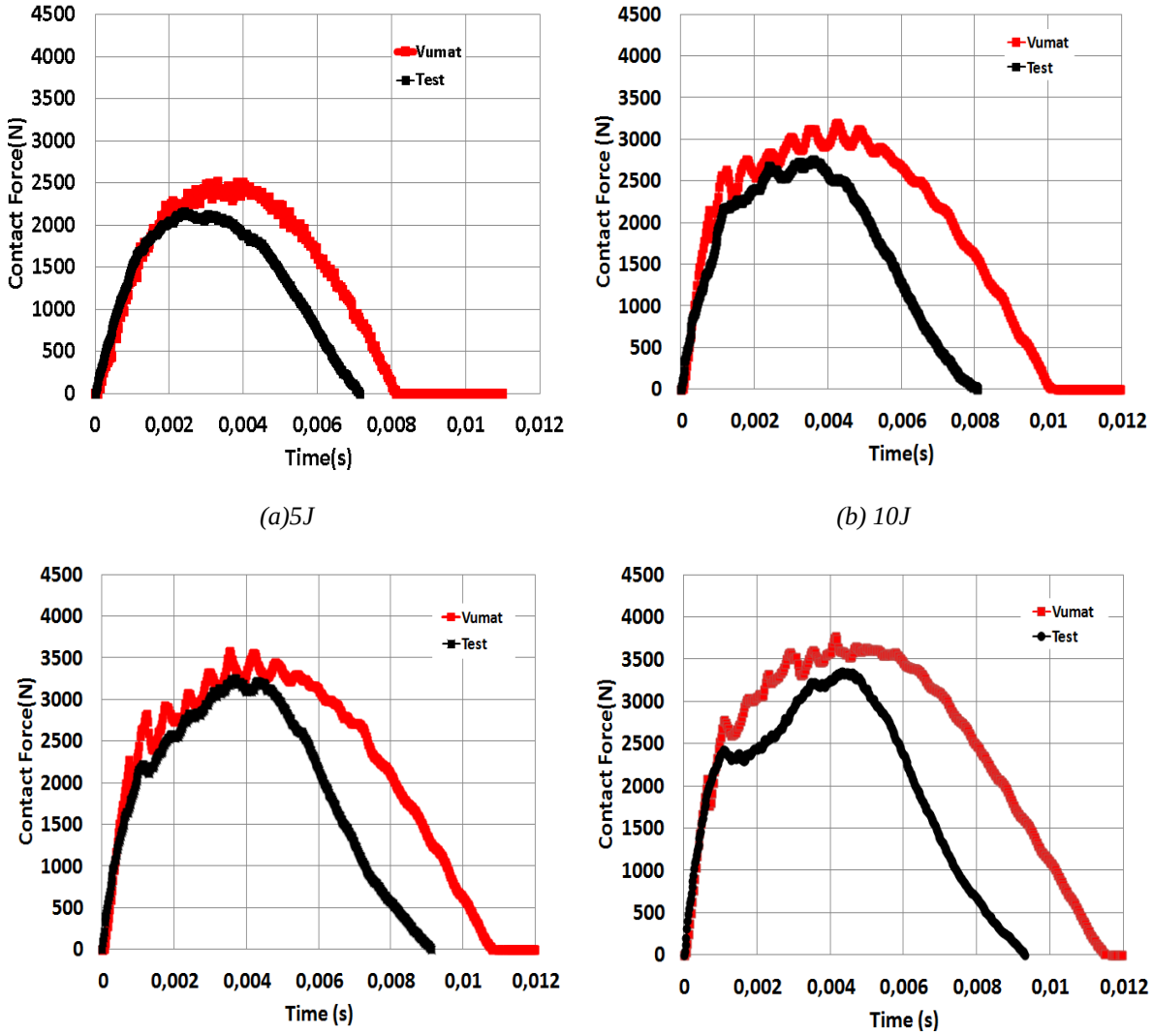

Fig. 10. Confrontation Test/3D simulation of contact force-time curves of stacking sequences GGC under different impact

Figs. 11, 12 and 13 compare the impactor displacements for the different implemented criteria. The numerical results show reasonable comparable trends with the filtered experimental curves and a similar temporal evolution, but overestimate the value of the displacements of the impactor in rebound and for the majority of cases, were observed. It can be noted that the stiffness predicted by the numerical model of the CGG and GCG configurations is higher than that given by the experimental results. This can be explained by the fact that in the numerical model, the interweaving of the fibres and their distribution is assumed to be perfect, whereas for the samples tested this is not guaranteed. In addition, when the criterion is verified numerically for certain elements, this results in their deletion, whereas physically these elements are still present [49], which may explain the overestimation of the contact forces for certain impact energies. In general, the model implemented with the three-dimensional criterion of Hashin (1980) (criterion presented) seems able to reproduce the overall behaviour.

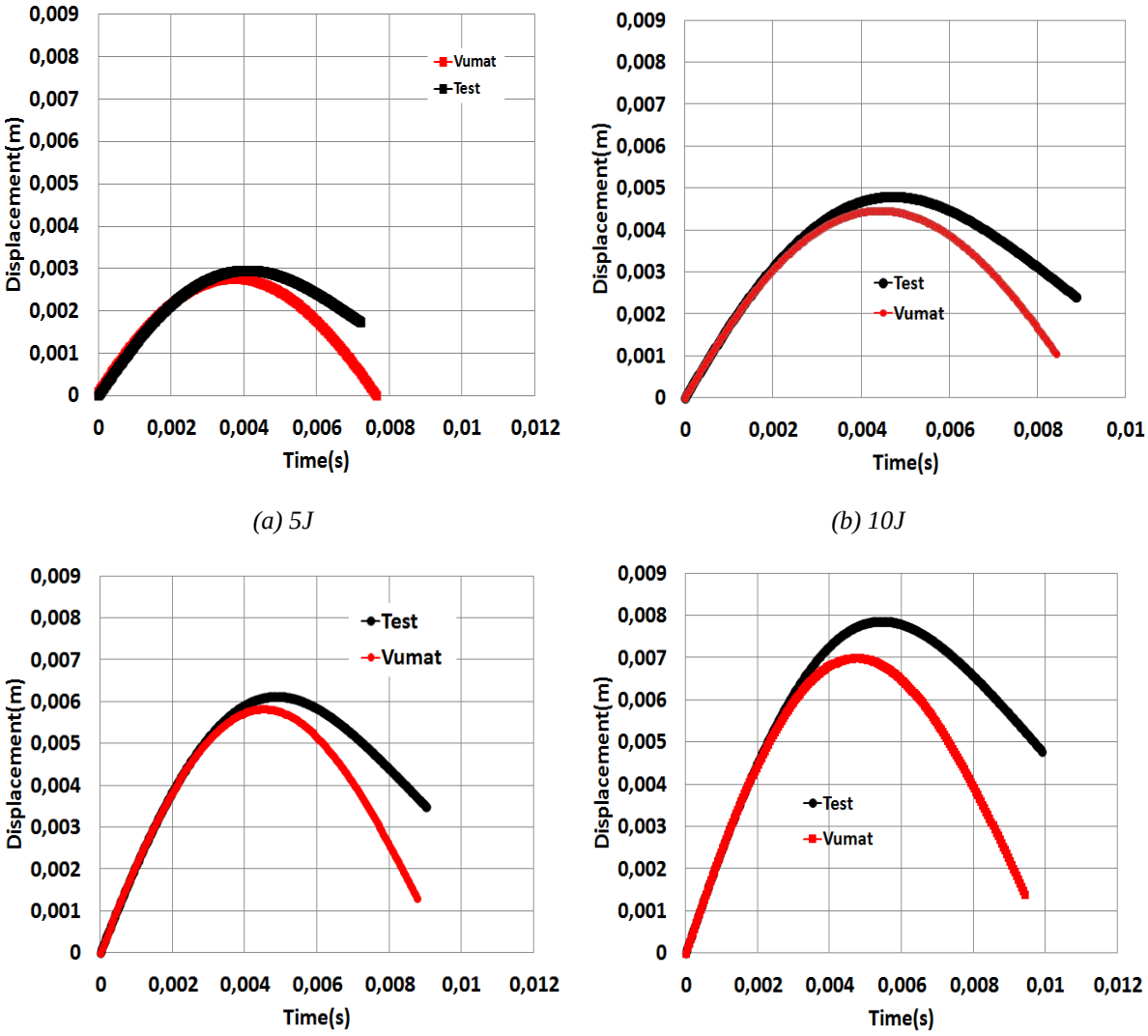

(a) 5J

(b) 10J

(c) 15J

(d) 20J

Fig. 11. Confrontation Test/3D simulation of displacement-time curves of stacking sequences CGG under different impact energy

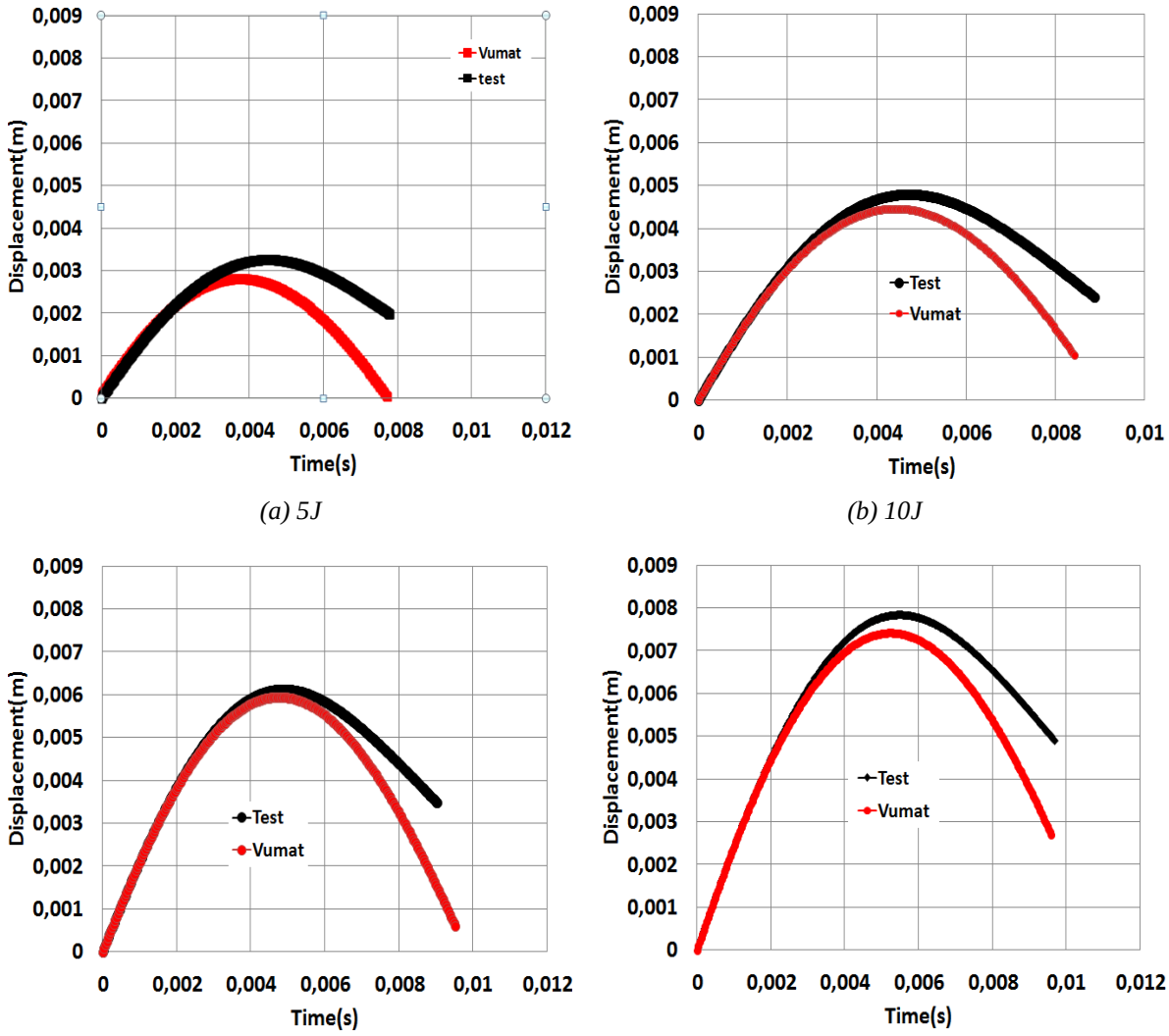

(a) 5J

(b) 10J

(c) 15J

(d) 20J

Fig. 12. Confrontation Test/3D simulation of displacement-time curves of stacking sequences GCG under different impact energy

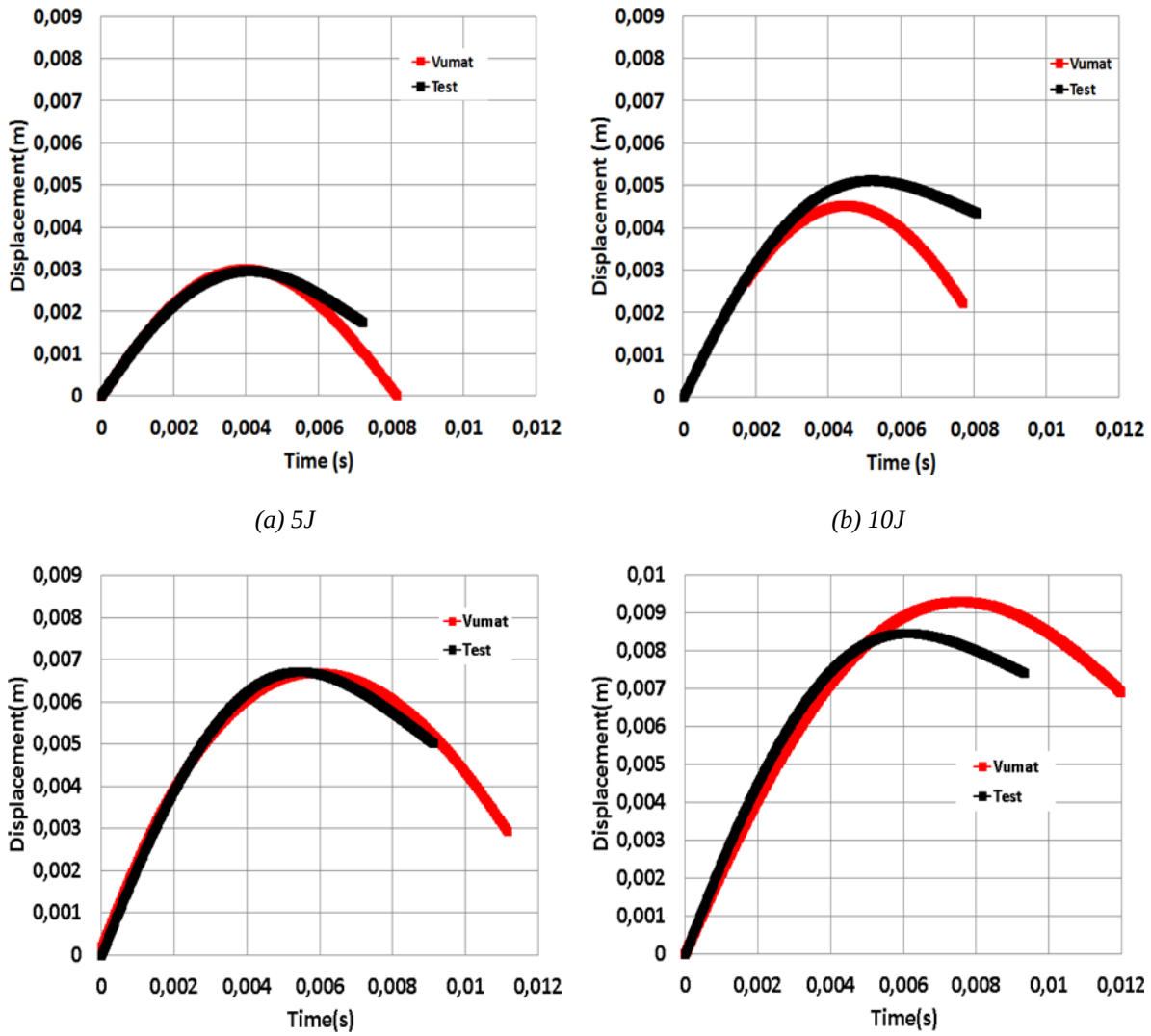

(a) 5J *(b) 10J*

(c) 15J *(d) 20J*

Fig. 13. Confrontation Test/3D simulation of displacement-time curves of stacking sequences GGC under different impact energy

4.1. Energy dissipation

The 3D models were capable to predict the absorbed energy evolution. The comparison between obtaining numerical results and experimental curve data at two cases 15J and 20J for different stacking sequences as shown in Fig. 14 is done. The stacking sequence GGC presents the highest energy absorption and the lowest rebound energy. In general, a small discrepancy between numerical and experimental curves was observed. For the impacted surface, the evaluated envelopes of the matrix cracking (Figs. 15, 16 and 17) subsequently the predicted behaviour. Matrix cracks produced in the way of the fibre direction. Delamination of each stacking sequences is reported in Fig. 20 at each interface (between two oriented plies) with affecting three different cohesive elements (glass-glass and glass-carbon and carbon-carbon) and it was not possible to compare with experimental

delamination due to the method of SEM used in the experimental investigation [26], the estimations by simulations for three stacking sequences are poorly overestimated. The overall interlaminar and intralaminar damage presents.

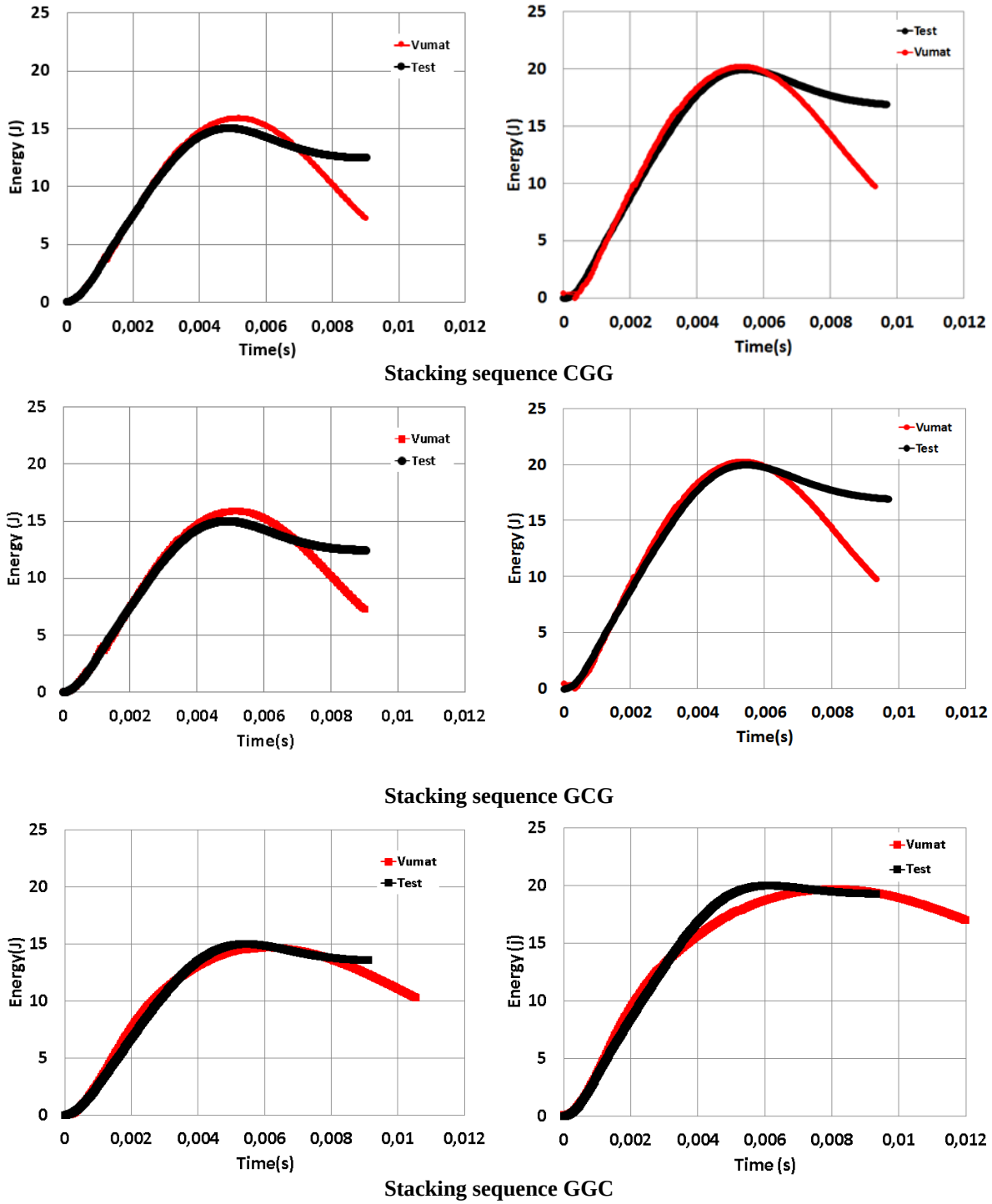

Fig. 14. Confrontation Test/3D simulation of energy-time curves of stacking layers CGG and GCG and GGC under two impact energy a) 15 J b) 20 J

A reasonable trend with a slight overestimation of the whole size. These overestimations of the simulations can be explained by several factors. The deficiency of details on interlaminar toughness could have consequences on the entire delaminated area. Overestimation of matrix cracks can be caused by the numerical model material

properties used for the simulation. The material properties of the fibres and matrix were measured on the same components and the same production process and some properties calculated or assumed, but with different production parameters. The properties of the cohesive zone model some adopted in literature, this could have influenced the values that reduced the accuracy of the model. Furthermore, the thickness was defined as the average value of the estimated value for samples.

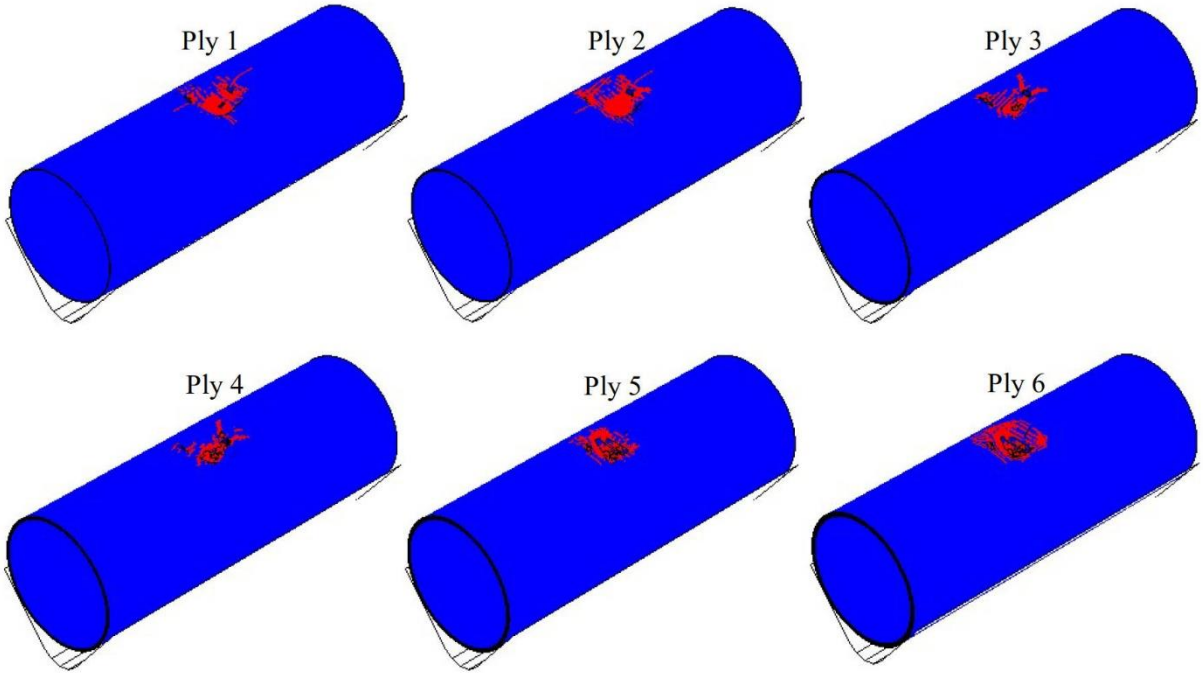

Fig. 15. Prediction of damage in a matrix for each ply of hybrid composite pipe under 20J impact energy (stacking GGC)

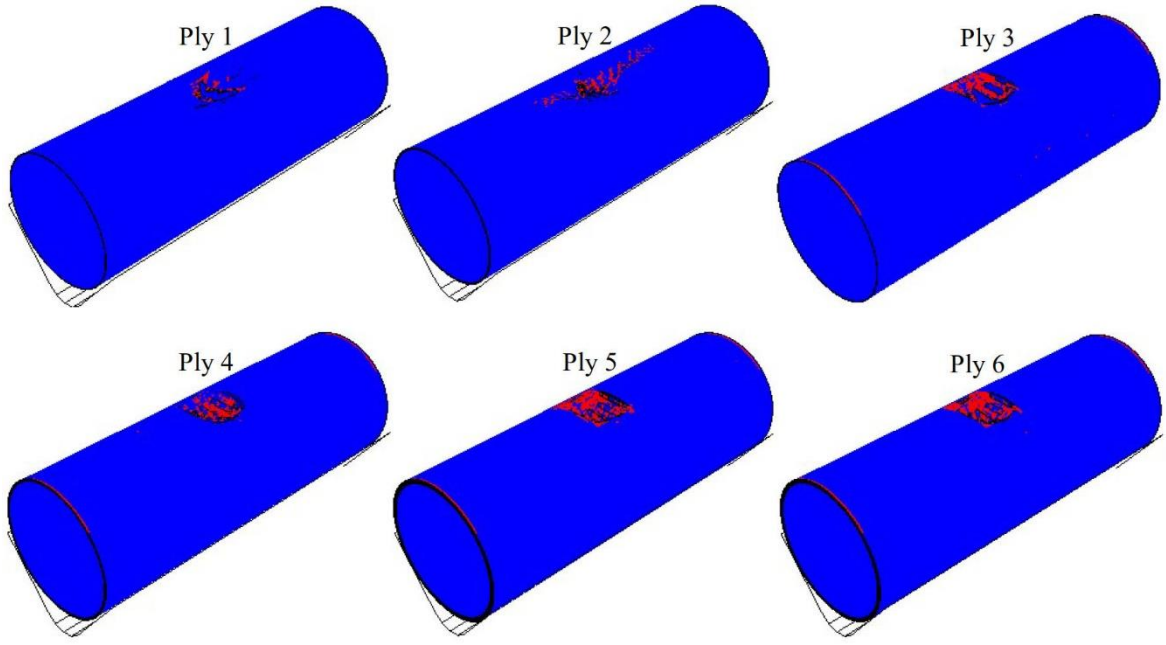

Fig. 16. Prediction of damage in a matrix for each ply of hybrid composite pipe under 20J impact energy (stacking GCG)

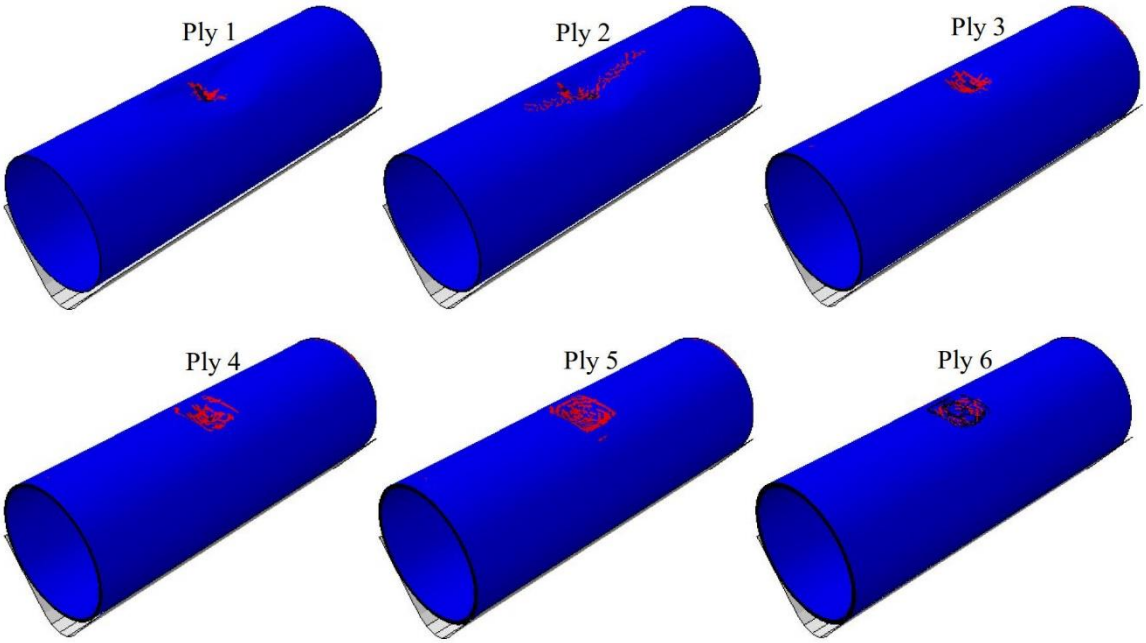

Fig. 17. Prediction of damage in a matrix for each ply of hybrid composite pipe under 20J impact energy (stacking CGG)

4.2. Damage formation

In this part, the progressive damage observed in pressurized hybrid composite pipe samples under low-velocity impact is presented. The damage formations and how were pictures taken and evaluated are shown in Fig. 18 which shows the damage formation of GGC specimen experimented under 20J energy level. For a better presentation of the damage formation with a clear comparison between the samples, damage analysis is focused on samples impacted at 20J. SEM figures captured in radial cross-section of CGG, GCG and GGC hybrid samples impacted at 20J energy level. Whereas the hybrid specimens pressurized at 32 bar internal pressure. SEM captures of each pressurized sample (CGG, GCG and GGC) subjected to low-velocity impact loading under 20J are presented in Figs. 19 and 20.

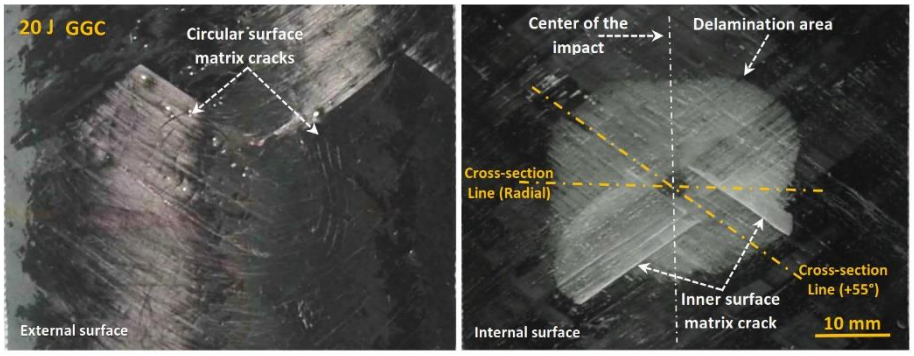

Fig. 18. Macro damage at GGC stacking hybrid composite pipe after low-velocity impact

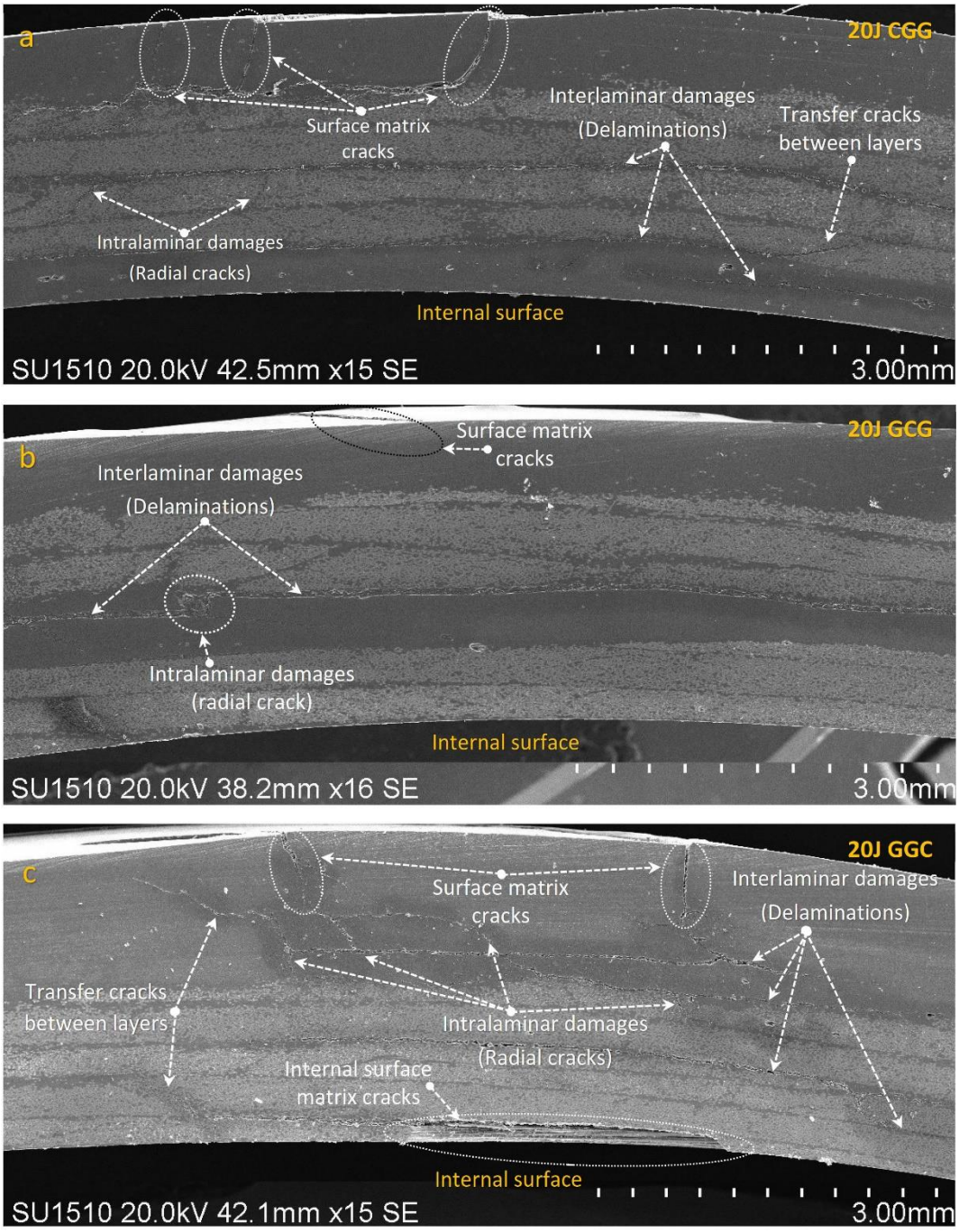

Fig. 19. SEM analysis of delamination damages after experimental work through the thickness of the hybrid composite pipe

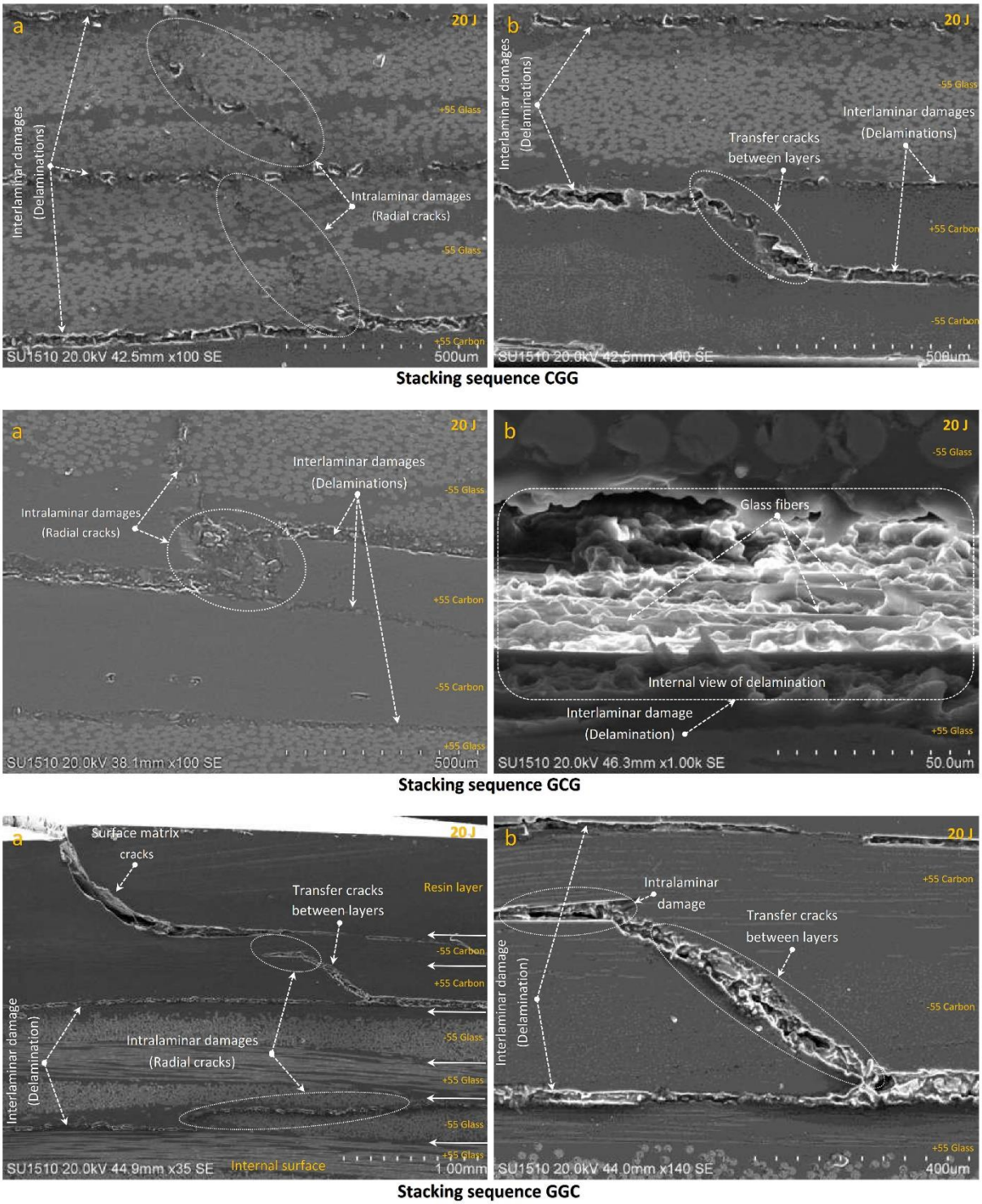

Fig. 20. Damages (intralaminar and interlaminar) after experimental work in hybrid composite pipes

In Fig. 21, cross-sectional images taken from the impact center and outside the impact center are given. When these images obtained in the numerical model are examined, although the displacement is the highest in the impact center, it is seen that the movement between the layers is low. On the contrary, the shear stresses formed by the effect of the displacement between the layers around the impact center significantly increased the delamination

damage. When Fig. 19, Fig. 20 and Fig. 21 are examined together, it is understood that the damages in low velocity impact are displacement controlled and especially the damages are concentrated around the impact center. When an evaluation is made according to the stacking sequence, delamination damage is seen extensively in GCG samples, while delamination and all other damage modes can be seen in GGC and CGG samples. Especially in the GGC sample, surface matrix cracks, interlayer transfer cracks, intralaminar damages (radial cracks) and internal surface matrix cracks were observed intensively. Considering these damage developments, it is seen that the stacking sequence of hybrid composite pipes significantly affects the damage development in low velocity impact response. In this study, after experimental and numerical investigations, it can be said that the GCG stacking is the most suitable design in terms of damage development in hybrid pipes followed by CGG, and GGC, respectively.

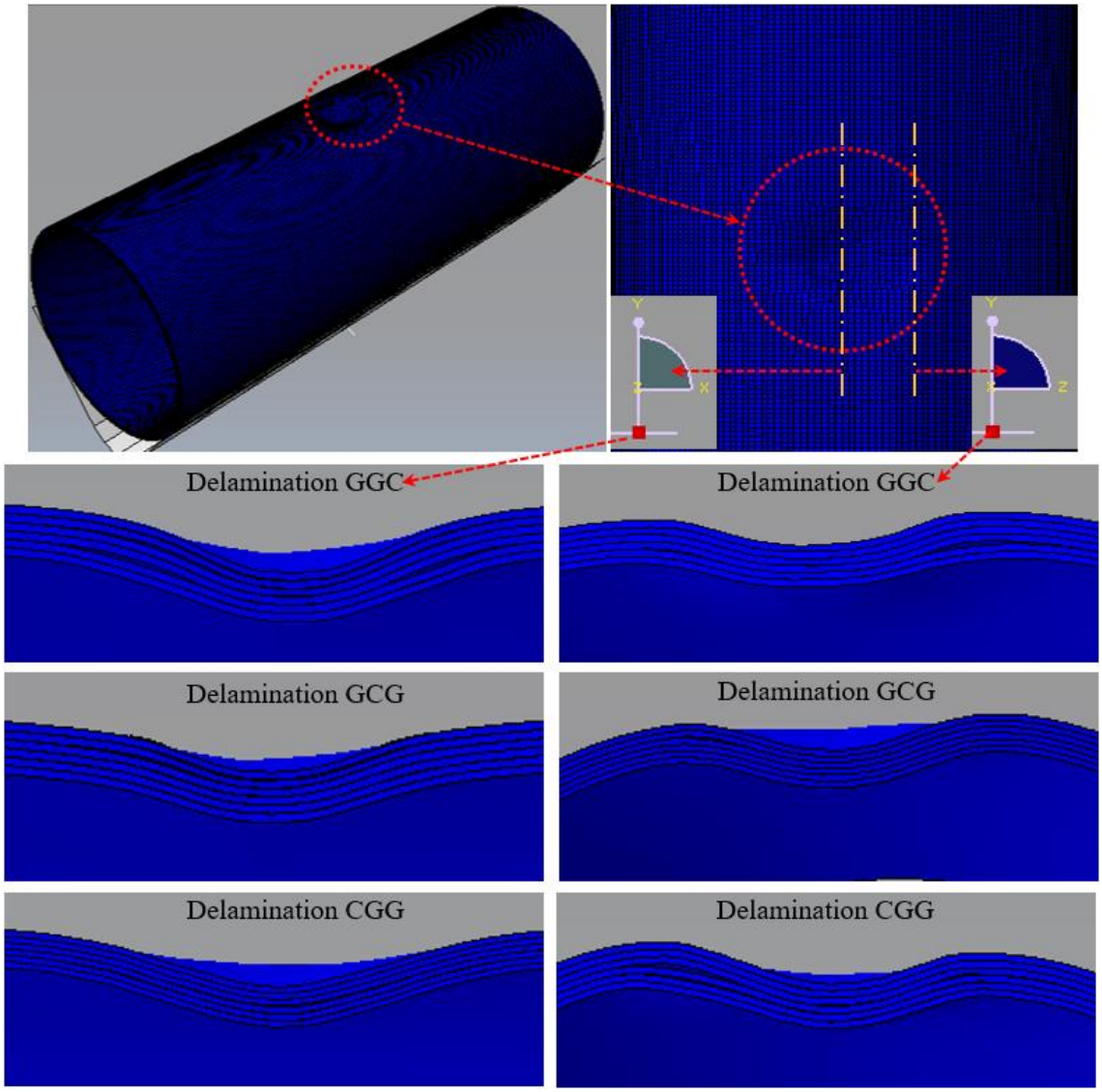

Fig. 21. Delamination predicted by the numerical model through the thickness of the hybrid composite pipe

Overall, the 3D model impact results (force-time, displacement-time, and energy-time reported) present the best agreement with the data of experimental investigation [26], indicating that, the formation of damage was modelled with enough accuracy. Alternatively work would be necessary to achieve a more accurate evaluation of the matrix cracks and delamination. More characterization should evaluate the composite material properties calculated/using in this study. Particular tests should be accomplished on the hybrid composite pipe to predict each material data.

5. Conclusions

Low-velocity impacts on pressurized full-scale hybrid composite pipe were numerically investigated. A 3D FE model is developed using both intralaminar and interlaminar damages theories. Hashin failure criteria were adopted to predict fibre failure and matrix cracking.

- Delamination onset events and propagation were simulated with the use of cohesive elements. The developed model was modelled in the FE Explicit/Abaqus software [57] by the implementation of a user-defined subroutine VUMAT. The model demonstrated the ability to predict the impact scenarios.
- The impact time evolution and the maximum impact load were predicted for different stacking sequences (Carbon-Glass-Glass, Glass-Carbon-Glass, Glass-Glass-Carbon) and validating using highly detailed experimental investigation published [26].
- The estimated displacement–time traces correlate well with experimental results in loading event. The increase of impact energy can promote the damage accumulation, and the implementation of progressive damage model governed by elements deletion when the criterion it will be satisfied plays a role in the difference between the numerical and experimental curves of impactor displacement in unloading events.
- A comparison of energy absorbed of three stacking sequences obtained by numerical model and experimental data is conducted and correlate well.
- The induced damage and the captures of each shape of matrix cracking and delamination was over calculated and predicted by the robust numerical simulation. The believed rationale for this small difference can be based on the lack of precision in the values of the used material properties, geometrical inaccuracy (thickness variation).

- Future work should focus on the mechanical characterization of hybrid composite laminate to evaluate the composite material properties. Overall the 3D FE model and the choice of failure criteria presented acceptable for modelling all scenarios of damage formation on a full-scale hybrid composite pipe.
- The study of the damage formation of the hybrid composite pipe under various loading events including low-velocity impact and internal pressure loads has all its interest to the designer. Indeed, even a very small initiating damage becomes a considerable cause of the degradation in the structural integrity of the hybrid composite structures.

References

[1] Abu Bakar MS, Salit MS, Mohamad Yusoff MZ, Zainudin ES, Ya HH. The crashworthiness performance of stacking sequence on filament wound hybrid composite energy absorption tube subjected to quasi-static compression load. Journal of Materials Research and Technology. 2020;9:654-66.

[2] Gemi L, Köroğlu MA, Ashour A. Experimental study on compressive behavior and failure analysis of composite concrete confined by glass/epoxy ±55° filament wound pipes. Composite Structures. 2018;187:157-68.

[3] Gemi L, Morkavuk S, Köklü U, Gemi DS. An experimental study on the effects of various drill types on drilling performance of GFRP composite pipes and damage formation. Composites Part B: Engineering. 2019;172:186-94.

[4] Gemi L, Tarakçioğlu N, Akdemir A, Şahin ÖS. Progressive fatigue failure behavior of glass/epoxy (±75)2 filament-wound pipes under pure internal pressure. Materials & Design. 2009;30:4293-8.

[5] Huang Z, Qian X, Su Z, Pham DC, Sridhar N. Experimental investigation and damage simulation of large-scaled filament wound composite pipes. Composites Part B: Engineering. 2020;184:107639.

[6] Tarfaoui M, Gning PB, Collombet F. Damage Modelling of Impacted Tubular Structures by Using Material Property Degradation Approach. Damage and Fracture Mechanics. Dordrecht: Springer Netherlands; 2009. p. 227-35.

[7] Kangal S, Kartav O, Tanoğlu M, Aktaş E, Artem HS. Investigation of interlayer hybridization effect on burst pressure performance of composite overwrapped pressure vessels with load-sharing metallic liner. Journal of Composite Materials. 2020;54:961-80.

[8] Mahdavi H, Rahimi GH, Farrokhabadi A. Fatigue Performance Analysis of GRE Composite Pipes by Conducting Tension-Tension Tests on the Rings Cut from the Pipe. 2019:2767-78.

[9] Manoj Prabhakar M, Rajini N, Ayrilmis N, Mayandi K, Siengchin S, Senthilkumar K, et al. An overview of burst, buckling, durability and corrosion analysis of lightweight FRP composite pipes and their applicability. Composite Structures. 2019;230:111419.

[10] Özbek Ö, Bozkurt ÖY. Hoop tensile and compression behavior of glass-carbon intraply hybrid fiber reinforced filament wound composite pipes. Materials Testing. 2019;61:763-9.

[11] Rafiee R. Experimental and theoretical investigations on the failure of filament wound GRP pipes. Composites Part B: Engineering. 2013;45:257-67.

[12] Rafiee R. On the mechanical performance of glass-fibre-reinforced thermosetting-resin pipes: A review. Composite Structures. 2016;143:151-64.

[13] Rafiee R, Reshadi F. Simulation of functional failure in GRP mortar pipes. Composite Structures. 2014;113:155-63.

[14] Benyahia H, Tarfaoui M, El Moumen A, Ouinas D, Hassoon OH. Mechanical properties of offshoring polymer composite pipes at various temperatures. Composites Part B: Engineering. 2018;152:231-40.

[15] Sebaey TA. Design of Oil and Gas Composite Pipes for Energy Production. Energy Procedia. 2019;162:146-55.

[16] Shabani P, Taheri-Behrooz F, Maleki S, Hasheminasab M. Life prediction of a notched composite ring using progressive fatigue damage models. Composites Part B: Engineering. 2019;165:754-63.

[17] Tarakçioğlu N, Gemi L, Yapici A. Fatigue failure behavior of glass/epoxy ±55 filament wound pipes under internal pressure. Composites Science and Technology. 2005;65:703-8.

[18] Uyaner M, Kara M, Gemi L. Filaman sarım E-camı/epoksi kompozit boruların düşük hızlı darbe sonrası mukavemeti. 13th International Materials Symposium (IMSP'2010) 2010. p. 644-52.

[19] Sahin ÖS, Akdemir A, Avci A, Gemi L. Fatigue Crack Growth Behavior of Filament Wound Composite Pipes in Corrosive Environment. Journal of Reinforced Plastics and Composites. 2009;28:2957-70.

[20] Gemi L, Köklü U, Yazman Ş, Morkavuk S. The effects of stacking sequence on drilling machinability of filament wound hybrid composite pipes: Part-1 mechanical characterization and drilling tests. Composites Part B: Engineering. 2020;186:107787.

[21] Gemi L, Morkavuk S, Köklü U, Yazman Ş. The effects of stacking sequence on drilling machinability of filament wound hybrid composite pipes: Part-2 damage analysis and surface quality. Composite Structures. 2020;235:111737.

[22] Madenci E, Özkılıç YO, Gemi L. Experimental and theoretical investigation on flexure performance of pultruded GFRP composite beams with damage analyses. Composite Structures. 2020;242:112162.

[23] Tarfaoui M, Gning PB, Hamitouche L. Dynamic response and damage modeling of glass/epoxy tubular structures: Numerical investigation. Composites Part A: Applied Science and Manufacturing. 2008;39:1-12.

[24] Rafiee R, Amini A. Modeling and experimental evaluation of functional failure pressures in glass fiber reinforced polyester pipes. Computational Materials Science. 2015;96:579-88.

[25] Farhood NH, Karuppanan S, Ya HH, Ovinis M. Effects of Carbon Fiber Hybridization on the Compressive Strength of Glass-Carbon/Epoxy Hybrid Composite Pipes before and after Low Velocity Impact. Key Engineering Materials. 2019;796:30-7.

[26] Gemi L. Investigation of the effect of stacking sequence on low velocity impact response and damage formation in hybrid composite pipes under internal pressure. A comparative study. Composites Part B: Engineering. 2018;153:217-32.

[27] Rafiee R, Ghorbanhosseini A, Rezaee S. Theoretical and numerical analyses of composite cylinders subjected to the low velocity impact. Composite Structures. 2019;226:111230.

[28] Rafiee R, Torabi MA, Maleki S. Investigating structural failure of a filament-wound composite tube subjected to internal pressure: Experimental and theoretical evaluation. Polymer Testing. 2018;67:322-30.

[29] Muflikhun MA, Higuchi R, Yokozeki T, Aoki T. The evaluation of failure mode behavior of CFRP/Adhesive/SPCC hybrid thin laminates under axial and flexural loading for structural applications. Composites Part B: Engineering. 2020;185:107747.

[30] Gemi L. Düşük hızlı darbe hasarlı filaman sarım hibrid boruların iç basınç altında yorulma davranışı. Ph.D Thesis, Konya-Turkey: Selçuk University 2014.

[31] Madenci E, Onuralp Özkılıç Y, Gemi L. Buckling and free vibration analyses of pultruded GFRP laminated composites: Experimental, numerical and analytical investigations. Composite Structures. 2020;254:112806.

[32] Gemi L, Kara M, Avci A. Low velocity impact response of prestressed functionally graded hybrid pipes. Composites Part B: Engineering. 2016;106:154-63.

[33] Gemi L, Sinan Şahin Ö, Akdemir A. Experimental investigation of fatigue damage formation of hybrid pipes subjected to impact loading under internal pre-stress. Composites Part B: Engineering. 2017;119:196-205.

[34] El Moumen A, Tarfaoui M, Hassoon O, Lafdi K, Benyahia H, Nachtane M. Experimental Study and Numerical Modelling of Low Velocity Impact on Laminated Composite Reinforced with Thin Film Made of Carbon Nanotubes. Applied Composite Materials. 2018;25:309-20.

[35] Mahdi E, Hamouda AMS, Sahari BB, Khalid YA. Effect of hybridisation on crushing behaviour of carbon/glass fibre/epoxy circular–cylindrical shells. Journal of Materials Processing Technology. 2003;132:49-57.

[36] Mousavi MV, Khoramishad H. The effect of hybridization on high-velocity impact response of carbon fiber-reinforced polymer composites using finite element modeling, Taguchi method and artificial neural network. Aerospace Science and Technology. 2019;94:105393.

[37] Zuraida A, Khalid AA, Ismail AF. Performance of hybrid filament wound composite tubes subjected to quasi static indentation. Materials & Design. 2007;28:71-7.

[38] Maziz A, Rechak S, Tarfaoui M. Comparative study of tubular composite structure subjected to internal pressure loading: Analytical and numerical investigation. Journal of Composite Materials. 2021;55:1517-33.

[39] Benyahia H, Tarfaoui M, Datsyuk V, El Moumen A, Trotsenko S, Reich S. Dynamic properties of hybrid composite structures based multiwalled carbon nanotubes. Composites science and technology. 2017;148:70-9.

[40] Gning PB, Tarfaoui M, Collombet F, Davies P. Prediction of Damage in Composite Cylinders After Impact. Journal of Composite Materials. 2005;39:917-28.

[41] Gning PB, Tarfaoui M, Collombet F, Riou L, Davies P. Damage development in thick composite tubes under impact loading and influence on implosion pressure: experimental observations. Composites Part B: Engineering. 2005;36:306-18.

[42] Tarfaoui M, Gning PB, Davies P, Collombet F. Scale and Size Effects on Dynamic Response and Damage of Glass/Epoxy Tubular Structures. Journal of Composite Materials. 2007;41:547-58.

[43] Özbek Ö, Bozkurt ÖY, Erkliğ A. An experimental study on intraply fiber hybridization of filament wound composite pipes subjected to quasi-static compression loading. Polymer Testing. 2019;79:106082.

[44] Guo W, Xue P, Yang J. Nonlinear progressive damage model for composite laminates used for low-velocity impact. Applied Mathematics and Mechanics. 2013;34:1145-54.

[45] Nachtane M, Tarfaoui M, El Moumen A, Saifaoui D. Damage prediction of horizontal axis marine current turbines under hydrodynamic, hydrostatic and impacts loads. Composite Structures. 2017;170:146-57.

[46] Nachtane M, Tarfaoui M, Saifaoui D, El Moumen A, Hassoon OH, Benyahia H. Evaluation of durability of composite materials applied to renewable marine energy: Case of ducted tidal turbine. Energy Reports. 2018;4:31-40.

[47] Laaouidi H, Tarfaoui M, Nachtane M, Trihi M. Energy absorption characteristics in hybrid composite materials for marine applications under impact loading: Case of tidal current turbine. International Journal of Energy Research. 2021;45:5894-911.

[48] Tarfaoui M, Gning PB, Collombet F. Residual Strength of Damaged Glass/Epoxy Tubular Structures. Journal of Composite Materials. 2007;41:2165-82.

[49] Shi Y, Swait T, Soutis C. Modelling damage evolution in composite laminates subjected to low velocity impact. Composite Structures. 2012;94:2902-13.

[50] Zhou J, Wen P, Wang S. Finite element analysis of a modified progressive damage model for composite laminates under low-velocity impact. Composite Structures. 2019;225:111113.

[51] Zhou J, Wen P, Wang S. Numerical investigation on the repeated low-velocity impact behavior of composite laminates. Composites Part B: Engineering. 2020;185:107771.

[52] Hassoon OH, Tarfaoui M, El Moumen A, Qureshi Y, Benyahia H, Nachtane M. Mechanical performance evaluation of sandwich panels exposed to slamming impacts: Comparison between experimental and SPH results. Composite Structures. 2019;220:776-83.

[53] Hassoon OH, Tarfaoui M, El Moumen A. Progressive damage modeling in laminate composites under slamming impact water for naval applications. Composite Structures. 2017;167:178-90.

[54] Hassoon OH, Tarfaoui M, El Malki Alaoui A. An experimental investigation on dynamic response of composite panels subjected to hydroelastic impact loading at constant velocities. Engineering Structures. 2017;153:180-90.

[55] Abrate S. Modeling of impacts on composite structures. Composite Structures. 2001;51:129-38.

[56] Aymerich F, Dore F, Priolo P. Simulation of multiple delaminations in impacted cross-ply laminates using a finite element model based on cohesive interface elements. Composites science and technology. 2009;69:1699-709.

[57] Lapczyk I, Hurtado JA. Progressive damage modeling in fiber-reinforced materials. Composites Part A: Applied Science and Manufacturing. 2007;38:2333-41.

[58] Xin SH, Wen HM. A progressive damage model for fiber reinforced plastic composites subjected to impact loading. International Journal of Impact Engineering. 2015;75:40-52.

[59] Hashin Z. Failure Criteria for Unidirectional Fiber Composites. Journal of Applied Mechanics. 1980;47:329-34.

[60] Singh H, Mahajan P. Modeling damage induced plasticity for low velocity impact simulation of three dimensional fiber reinforced composite. Composite Structures. 2015;131:290-303.

[61] Benzeggagh ML, Kenane M. Measurement of mixed-mode delamination fracture toughness of unidirectional glass/epoxy composites with mixed-mode bending apparatus. Composites science and technology. 1996;56:439-49.

[62] Tarfaoui M, El Moumen A, Lafdi K. Progressive damage modeling in carbon fibers/carbon nanotubes reinforced polymer composites. Composites Part B: Engineering. 2017;112:185-95.

[63] Lancaster JK. The effect of carbon fibre reinforcement on the friction and wear of polymers. Journal of Physics D: Applied Physics. 1968;1:549-59.

[64] Schön J. Coefficient of friction of composite delamination surfaces. Wear. 2000;237:77-89.

[65] Taşyürek M, Kara M. Low-velocity impact response of pre-stressed glass fiber/nanotube filled epoxy composite tubes. Journal of Composite Materials. 2021;55:915-26.

[66] Kara M, Uyaner M, Avci A, Akdemir A. Effect of non-penetrating impact damages of pre-stressed GRP tubes at low velocities on the burst strength. Composites Part B: Engineering. 2014;60:507-14.

[67] AWWA A. C950-07–AWWA Standard for fiberglass pressure pipes–American Water Works Association. 6666 W Quincy Ave, Denver, Colorado, USA. 2006.

[68] Rafiee R, Fakoor M, Hesamsadat H. The influence of production inconsistencies on the functional failure of GRP pipes. Steel and Composite Structures. 2015;19:1369-79.

[69] Sari M, Karakuzu R, Deniz ME, Icten BM. Residual failure pressures and fatigue life of filament-wound composite pipes subjected to lateral impact. Journal of Composite Materials. 2012;46:1787-94.

[70] Kara M, Uyaner M, Avci A. Repairing impact damaged fiber reinforced composite pipes by external wrapping with composite patches. Composite Structures. 2015;123:1-8.

[71] Kara M, Kırıcı M, Tatar AC, Avcı A. Impact behavior of carbon fiber/epoxy composite tubes reinforced with multi-walled carbon nanotubes at cryogenic environment. Composites Part B: Engineering. 2018;145:145-54.

[72] Kara M, Kırıcı M. Effects of the number of fatigue cycles on the impact behavior of glass fiber/epoxy composite tubes. Composites Part B: Engineering. 2017;123:55-63.

[73] Deniz ME, Ozen M, Ozdemir O, Karakuzu R, Icten BM. Environmental effect on fatigue life of glass–epoxy composite pipes subjected to impact loading. Composites Part B: Engineering. 2013;44:304-12.

[74] Deniz ME, Ozdemir O, Ozen M, Karakuzu R. Failure pressure and impact response of glass–epoxy pipes exposed to seawater. Composites Part B: Engineering. 2013;53:355-61.

[75] Gemi L, Kayrıcı M, Uludağ M, Gemi DS, Şahin ÖS. Experimental and statistical analysis of low velocity impact response of filament wound composite pipes. Composites Part B: Engineering. 2018;149:38-48.

[76] Gemi DS, Gemi L, Şahin ÖS. Investigation of Low Velocity Impact Response of (Ø54, $(\pm 55)_3$) GRP Composite Pipes. The International Alumınıum-Themed Engineering and Natural Sciences Conference (IATENS'19). Seydişehir/TURKEY-2019. p. 309-12.

[77] Gemi DS. Filaman sarım CTP borularda darbe sonrası basma (CAI) davranışının incelenmesi Konya Teknik Üniversitesi, Lisansüstü Eğitim Enstitüsü, Konya, 2019.

[78] Maziz, A., Tarfaoui, M., Rechak, S., Nachtane, M., & Gemi, L. (2021). Finite element analysis of impact-induced damage in pressurized hybrid composites pipes. International Journal of Applied Mechanics, 13(07), 2150074.

[79] Gemi, D. S., Şahin, Ö. S., & Gemi, L. (2021). Experimental investigation of the effect of diameter upon low velocity impact response of glass fiber reinforced composite pipes. Composite Structures, 275, 114428.